



UNIVERSITEIT•STELLENBOSCH•UNIVERSITY
jou kennisvennoot • your knowledge partner

Virtual Object Reconstruction from Paired-Point Distances

Emile Visser

21595240

Report submitted in partial fulfilment of the requirements of the module
Project (E) 448 for the degree Baccalaureus in Engineering in the Department of
Electrical and Electronic Engineering at Stellenbosch University.

Supervisor: Prof. J. du Preez

November 2021

Acknowledgements

I would like to extend my thanks to my supervisor, Prof. Johan du Preez, for his guidance and counsel. This report would not be possible without the knowledge and philosophy that he has graciously shared. To my family, friends and colleagues, thank you for your unwavering support. Finally, i would like to thank Frank Herbert for reassuring me that the fear will pass over me and through me, and where the fear has gone there will be nothing.

Only I will remain.



UNIVERSITEIT•STELLENBOSCH•UNIVERSITY
jou kennisvennoot • your knowledge partner

Plagiaatverklaring / Plagiarism Declaration

1. Plagiaat is die oorneem en gebruik van die idees, materiaal en ander intellektuele eiendom van ander persone asof dit jou eie werk is.

Plagiarism is the use of ideas, material and other intellectual property of another's work and to present it as my own.

2. Ek erken dat die pleeg van plagiaat 'n strafbare oortreding is aangesien dit 'n vorm van diefstal is.

I agree that plagiarism is a punishable offence because it constitutes theft.

3. Ek verstaan ook dat direkte vertalings plagiaat is.

I also understand that direct translations are plagiarism.

4. Dienooreenkomsdig is alle aanhalings en bydraes vanuit enige bron (ingesluit die internet) volledig verwys (erken). Ek erken dat die woordelikse aanhaal van teks sonder aanhalingstekens (selfs al word die bron volledig erken) plagiaat is.

Accordingly all quotations and contributions from any source whatsoever (including the internet) have been cited fully. I understand that the reproduction of text without quotation marks (even when the source is cited) is plagiarism

5. Ek verklaar dat die werk in hierdie skryfstuk vervat, behalwe waar anders aangedui, my eie oorspronklike werk is en dat ek dit nie vantevore in die geheel of gedeeltelik ingehandig het vir bepunting in hierdie module/werkstuk of 'n ander module/werkstuk nie.

I declare that the work contained in this assignment, except where otherwise stated, is my original work and that I have not previously (in its entirety or in part) submitted it for grading in this module/assignment or another module/assignment.

Studentenommer / Student number	Handtekening / Signature
Voorletters en van / Initials and surname	Datum / Date

Abstract

With the advent of autonomous agents such as vehicles, drones, etc., the need has arisen for a way to translate objects from the physical to virtual space. Modern computer vision algorithms can identify points on an object and calculate the distances between them, but have no way to represent these distances as an internal, virtual object. The aim of this research paper is to develop two algorithms that can solve the reconstruction from paired-point distances problem, even in the presence of measurement noise and corrupted measurement records.

The first of these two algorithms is a deterministic algorithm based on the theory of linear algebra and, in particular, the Euclidean distance matrix (EDM), multidimensional scaling (MDS) and semidefinite programming (SDP). In contrast, the second algorithm is developed probabilistically, using the theory of probabilistic graphical models (PGM) and the unscented transform (UT). This report contains both the respective theoretical backgrounds and the implementations used for the testing of the two algorithms.

After extensive testing, using data generated from a virtual reference object, it is clear that the probabilistic algorithm outperforms the baseline deterministic algorithm in most practical applications.

Uittreksel

Met die aankoms van outonome agente soos voertuie, hommeltuie, ens., die behoefde het onststaan vir 'n manier om voowerpe oor te bring van die fisiese na die virtuele ruimte. Modene rekenaarvisie-algoritmes kan punte identifiseer op 'n voorwerp en die afstande meet tussen hulle, maar het geen manier om hierdie afstandmetings as 'n interne, virtuele voorwerp voor te stel nie. Die mikpunt van hierdie verslag is om twee algoritmes te ontwerp om die rekonstruksie van paarpuntafstande probleem op te los, selfs in die teenwoordigheid van afmetingsruis en foutiewe afmetings.

Die eerste van hierdie twee algoritmes is 'n deterministiese metode gebaseer op die teorie van lineêre algebra en veral die *Euclidean distance matrix* (EDM), *multidimensional scaling* (MDS) en *semidefinite programming* (SDP). In teenstelling, word die tweede algoritme waarskynlikheidsgewys ontwikkel deur middel van *probabilistic graphical models* (PGM) en die *unscented transform* (UT). Hierdie verslag bevat beide die onderskeie agtergrondsteorie en implementerings word gebruik word vir die analise van die algoritmes.

Na omvattende toetse met data wat gegenereer is van 'n virtuele verwysingsvoorwerp, is dit duidelik dat die waarskynlikheidsgebaseerde algoritme die deterministiese algoritme oortref in meeste praktiese toepassings.

Contents

Declaration	ii
Abstract	iii
Uittreksel	iv
List of Figures	vii
List of Tables	ix
Nomenclature	x
1. Introduction	1
1.1. Objectives	1
1.2. Outcomes	2
1.3. Overview	2
2. Deterministic Reconstruction Methods	3
2.1. Euclidean Distance Matrix	4
2.2. Multidimensional Scaling	4
2.3. Semidefinite Programming	6
2.4. Rotation Matrix Estimation	8
2.4.1. Naive Inverse Matrix	8
2.4.2. Moore-Penrose Inverse Matrix	9
2.4.3. Kabsch Algorithm and Householder Matrix	9
2.5. Summary	11
3. Probabilistic Reconstruction Methods	12
3.1. Probabilistic Graphical Model	13
3.1.1. Bayes and Markov Networks	13
3.1.2. Gaussian Markov Random Fields	15
3.2. Unscented Transform	16
3.3. Positional Inference	19
3.3.1. Marginal Inference	19
3.3.2. Junction Tree Algorithm	19
3.3.3. Loopy Belief Propagation	20

3.4. Summary	21
4. Finding Erroneous Distance Measurements	22
4.1. Heuristic Identification	23
4.2. Probabilistic Identification	23
4.3. Summary	24
5. Experimental Setup	25
5.1. Dataset Generation	25
5.2. Deterministic Reconstruction Algorithm Implementation	26
5.3. Probabilistic Reconstruction Algorithm Implementation	27
5.4. Error Identification Heuristic Implementation	29
5.5. Result Visualisation	29
5.6. Error Quantification	31
6. Experimental Results	32
6.1. Deterministic Algorithm Performance	32
6.2. Probabilistic Algorithm Performance	34
6.3. Performance Comparison	38
7. Summary and Conclusion	39
7.1. Summary	39
7.2. Conclusion	40
7.3. Future Work	40
Bibliography	41
A. Project Planning Schedule	44
B. Outcomes Compliance	45
C. Matlab/CVX Script for Semidefinite Relaxation	46
D. Dataset Generation Algorithm Pseudocode	47
E. Deterministic Reconstruction Algorithm Pseudocode	48
F. Probabilistic Reconstruction Algorithm Pseudocode	50
G. Heuristic Error Identification Algorithm Pseudocode	52

List of Figures

2.1. Deterministic Reconstruction Method Flowchart	3
3.1. Probabilistic Reconstruction Method Flowchart	12
3.2. Equivalent Bayes and Markov Networks	14
3.3. Simplified Hyperplane Example	17
3.4. Simplified Unscented Transform with Observed Distance Example	18
3.5. Junction Tree and Cluster Graph of 6-bit Hamming Code	20
4.1. Heuristic Error Identification Method Flowchart	22
5.1. Reference Object and Surface Points for Testing	25
5.2. Deterministic Algorithm Error for Various Data Fidelity (λ) Values	26
5.3. Unrotated- and Rotated Deterministic Reconstructions	27
5.4. Simplified Probabilistic Algorithm Iteration Example	28
5.5. Scatter and Alpha Shape Plot Examples	30
5.6. Alpha Shapes with Suitable and Excessive Values for α	30
5.7. Reconstruction Behaviour Example	31
6.1. Error Surface and Line Graph for Network Interconnection and Measurement Noise Percentage with Deterministic Algorithm	33
6.2. Error Surface and Line Graph for Network Interconnection and Record Error Percentage with Deterministic Algorithm	33
6.3. Relative Error of Deterministic Algorithm after Removing Corrupted Records Identified by Heuristic Algorithm	34
6.4. Error Surface and Line Graph for Network Interconnection and Positional Prior Standard Deviation with Probabilistic Algorithm (1% Noise)	35
6.5. Error Surface and Line Graph for Network Interconnection and Positional Prior Standard Deviation with Probabilistic Algorithm (20% Noise)	35
6.6. Error Surface and Line Graph for Network Interconnection and Measurement Noise Percentage with Randomly Initialised Probabilistic Algorithm	36
6.7. Error Surface and Line Graph for Network Interconnection and Measurement Noise Percentage with Probabilistic Algorithm (Prior Standard Deviation = 100)	36

6.8. Error Surface and Line Graph for Network Interconnection and Record Error Percentage with Probabilistic Algorithm (Prior Standard Deviation $= 100$)	37
6.9. Relative Error of Probabilistic Algorithm after Removing Corrupted Records Identified by Heuristic Algorithm	37
6.10. Performance Comparison of Deterministic and Probabilistic Reconstruction Algorithms	38

List of Tables

5.1. Example Distance Measurements List	26
5.2. Example Prior/Result Positions List	28
A.1. Project Schedule per Week	44
B.1. ECSA Outcomes Compliance	45

Nomenclature

Variables and functions

n	Number of points in original set.
k	Dimension of points in original set.
\mathbf{x}_i	Original point with index i .
\mathbf{X}	Original set of points.
$\hat{\mathbf{X}}$	Reconstructed set of points.
\mathbf{D}	Fully defined Euclidean Distance Matrix of \mathbf{X} .
$\tilde{\mathbf{D}}$	Partially defined Euclidean Distance Matrix of \mathbf{X} .
\mathbf{W}	Mask matrix of partially defined Euclidean Distance Matix $\tilde{\mathbf{D}}$.
\mathbf{E}	Set of measurements in partially defined Euclidean Distance Matix $\tilde{\mathbf{D}}$.
$\hat{\mathbf{E}}$	Set of measurements from reconstructed set $\hat{\mathbf{X}}$ that correspond to the original set \mathbf{E} .
$\hat{\mathbf{D}}$	Reconstructed full Euclidean Distance Matrix of $\tilde{\mathbf{D}}$.
\mathbf{G}	Gram matrix.
\mathbf{C}	Geometric centering matrix.
$\mathcal{G}(\mathbf{D})$	Function returning Gram matrix of Euclidean Distance Matrix \mathbf{D} .
$\mathcal{K}(\mathbf{G})$	Function returning Euclidean Distance Matrix of Gram matrix \mathbf{G} .
\mathbf{I}_n	Identity matrix of size $n \times n$.
$\mathbf{1}_n$	Vector of ones of size $n \times 1$.
$\ \mathbf{x}\ _2$	L^2 norm of vector \mathbf{x} .
$\ \mathbf{X}\ _F$	Frobenius norm of matrix \mathbf{X} .
$\mathbf{X} \cdot \mathbf{Y}$	Dot product of matrices \mathbf{X} and \mathbf{Y} .
$\mathbf{X} \times \mathbf{Y}$	Cross product of matrices \mathbf{X} and \mathbf{Y} .
$\mathbf{X} \circ \mathbf{Y}$	Hadamard (element-wise) product of matrices \mathbf{X} and \mathbf{Y} .
\mathbf{X}^\top	Transpose of matrix \mathbf{X} .
\mathbf{X}^{-1}	Inverse of matrix \mathbf{X} .
\mathbf{X}^+	Moore-Penrose inverse of matrix \mathbf{X} .

$\det(\mathbf{X})$	Determinant of matrix \mathbf{X} .
$\text{tr}(\mathbf{X})$	Trace of matrix \mathbf{X} .
$\text{rank}(\mathbf{X})$	Rank of matrix \mathbf{X} .
$\text{EVD}(\mathbf{X})$	Eigenvalue Decomposition of matrix \mathbf{X} .
$\mathbb{R}^{x \times y}$	Space of real matrices of size $x \times y$.
\mathbb{R}_+^n	Space of positive semidefinite matrices of size $n \times n$.
\mathbb{S}_c^n	Space of symmetric, geometrically centered matrices of size $n \times n$.
EDM^n	Space of Euclidean Distance Matrices of size $n \times n$.
$O(n)$	Bachmann–Landau notation that describes the order of function n .
$\text{card}(\mathcal{A})$	Cardinality/Size of set \mathcal{A} .
a_j	Element j of sequence $(a_i)_{i=1}^{\text{card}(\mathcal{A})}$ of set \mathcal{A} .
$\text{sort}_{\text{asc}}(\mathcal{A} \mid \mathcal{B})$	Sort set \mathbf{A} based on values of set \mathbf{B} ($\text{card}(\mathcal{A}) = \text{card}(\mathcal{B})$).
Pa_X^G	Parents of random variable X in graph G .
$\boldsymbol{\mu}$	Statistical mean vector.
$\boldsymbol{\Sigma}$	Statistical covariance matrix.
$\mathbf{X} \sim \mathcal{N}(\boldsymbol{\mu}, \boldsymbol{\Sigma})$	Multivariate Gaussian PDF of multidimensional random variable \mathbf{X} with mean vector $\boldsymbol{\mu}$ and covariance matrix $\boldsymbol{\Sigma}$.

$$\text{sgn}(x) \stackrel{\text{def}}{=} \begin{cases} -1 & x < 0 \\ 0 & x = 0 \\ 1 & x > 0 \end{cases}$$

Acronyms and abbreviations

CPD	Conditional Probability Distribution
DAG	Directed Acyclic Graph
EDM	Euclidean Distance Matrix
EKF	Extended Kalman Filter
MAP	Maximum a Posteriori
MDS	Multidimensional Scaling
MRF	Markov Random Field
PCoA	Principal Coordinates Analysis
PGM	Probabilistic Graphical Model
RIP	Running Intersection Property
RMSE	Root Mean Squared Error
SDP	Semidefinite Programming
SVD	Singular Value Decomposition
UKF	Unscented Kalman Filter
UT	Unscented Transform

Chapter 1

Introduction

With the advent of autonomous agents such as vehicles and drones, the need has arisen for a way to translate observed objects from the physical to virtual space. Using these virtual objects, the autonomous agent can create an internal approximation of its surroundings that can be used for pathfinding, anomaly detection, etc.

Modern, state of the art computer vision algorithms use feature extraction algorithms to identify points on an arbitrary object. Alongside cameras in stereo, the approximate distances between these points can be calculated using homography. Using these distance measurements between pairs of identified features and little to no prior knowledge of the shape of the object, a virtual representation of the object must be constructed.

While this problem is relatively trivial in the case with complete, exact and correct measurements, in practice these measurements are subject to the performance of the feature extraction and homography algorithms, which may introduce noise, identify incorrect feature pairs or return an incomplete dataset.

This report seeks to address this problem by creating algorithms that are resilient against these errors while reconstructing the 3-D object from the paired distance measurements.

1.1. Objectives

The objectives identified for solving the reconstruction problem are given below:

- Assemble an algorithm based on standard deterministic methods to solve the reconstruction from paired-point distances problem. This algorithm will provide a performance baseline to compare the next algorithm against.
- Construct an algorithm based on probabilistic methods to solve the reconstruction from paired-point distances problem.
- Develop a method to determine anomalous measurements in the paired-point distances set.
- Test the two algorithms with varying hyperparameters (network interconnectivity, noise, distance error, etc.).

- Draw a conclusion on the relative performance of these two algorithms.

1.2. Outcomes

As seen in Sec. 6.3, the probabilistic algorithm developed in this report outperformed the baseline deterministic algorithm for most practical applications. The error identification algorithm also yielded marginal performance benefits when good amounts of data were available.

1.3. Overview

In summary, this report aims to solve the reconstruction from paired-point distances problem using algorithms that are based on deterministic- and probabilistic methods respectively.

The deterministic algorithm is developed, using the standard approach to this problem to serve as a performance comparison baseline, from the theory of Euclidean distance matrices (Sec. 2.1) to represent the observed distances, semidefinite programming (Sec. 2.3) to calculate the missing entries in this matrix and multidimensional scaling (Sec. 2.1) to map the reconstructed points from the completed matrix.

As an alternative solution to the baseline algorithm, the probabilistic algorithm is based on the theory of probabilistic graphical models (Sec. 3.1). In this model, belief regarding the positions of the reconstructed points is represented as probability distributions with these beliefs propagated across the model and readjusted using the unscented transform (3.2) to conform to the observed distances.

In order to improve reconstruction performance, distance measurements that have been corrupted are identified and removed using a heuristic (Sec. 4.1) based on the change between the original measurements and the distances between the reconstructed points.

The implementation of these algorithms are given in Sec. 5.2 though 5.4 with their testing framework for this report consisting of a reference set of points on the surface of a virtual cube. From this set of points a dataset of measurements can be generated according to a set of parameters such as the number of connections per point, noise and percentage of records corrupted (Sec. 5.1). Quantification of the reconstruction error is done by calculating the relative change between the Euclidean distance matrix of the reference- and reconstructed set of points (Sec. 5.6).

The performance of the algorithms when subjected to varying dataset parameters is given in Ch. 6 and from these results, conclusions are drawn regarding the relative performance of the algorithms.

Chapter 2

Deterministic Reconstruction Methods

Mentat computation remained finite. You couldn't say something boundless within the boundaries of any language. Mentat abilities had their uses, though.

— Paul Atreides, *Dune Messiah* [1]

This chapter is focused on solving the reconstruction problem deterministically (as opposed to the probabilistic methods of Ch. 3).

This chapter stands on the foundation of the Euclidean distance matrix (EDM) of Sec. 2.1, a matrix that describes the squared distance between every possible pair of points in the system. Using this matrix, multidimensional scaling (MDS) of Sec. 2.2 can be applied to reconstruct the least squares error map onto an arbitrary Cartesian space, in the physical case three-dimensional, up to translation, rotation and reflection.

MDS, however, requires a fully defined EDM, i.e. must contain distance information for every point to every other point. Therefore semidefinite programming (SDP), detailed in Sec. 2.3 is used to reconstruct the full EDM from a partially defined EDM.

Using a subset of known points, the MDS reconstruction can be rotated/reflected to align with the known points using the Householder matrix and Kabsch Algorithm (given in Sec. 2.4).

A flowchart describing this method is given in Fig. 2.1 below:

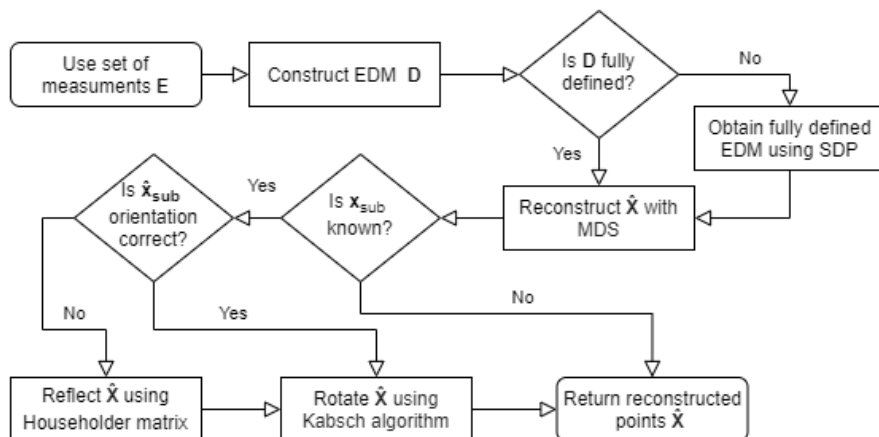


Figure 2.1: Deterministic Reconstruction Method Flowchart

2.1. Euclidean Distance Matrix

From Ch. 5 of *Convex Optimization & Euclidean Distance Geometry* [2], a Euclidean distance matrix (EDM) is defined as a \mathbb{R}_+^n matrix on the set of n, k dimensional points $\mathbf{X} = \{\mathbf{x}_i, i = 1 \dots n\}$ in $\mathbb{R}^{1 \times k}$ where element d_{ij} in the matrix is defined as the square of the L^2 norm (which is strictly smooth and convex as opposed to the L^1 norm which is non-smooth and convex [3]) of the difference between points x_i and x_j with noise ϵ :

$$d_{ij} = \|x_i - x_j\|_2^2 + \epsilon \quad \text{where } i, j \in \{1 \dots n\} \quad (2.1)$$

For example, in the case where $n = 3$:

$$\mathbf{D} = \begin{bmatrix} d_{11} & d_{12} & d_{13} \\ d_{21} & d_{22} & d_{23} \\ d_{31} & d_{32} & d_{33} \end{bmatrix} = \begin{bmatrix} 0 & d_{12} & d_{13} \\ d_{21} & 0 & d_{23} \\ d_{31} & d_{32} & 0 \end{bmatrix} \quad \text{since } d_{ij} = 0 \quad \text{where } i = j \quad (2.2)$$

A useful property of the EDM is that the symmetric Gram matrix \mathbf{G} obtained by applying the geometric centering matrix \mathbf{C} , is positive semidefinite [4]. This property is defined below and is used in Sec. 2.3.

$$\mathbf{C} \stackrel{\text{def}}{=} \mathbf{I}_n - \frac{1}{n} \mathbf{1}_n \mathbf{1}_n^\top \quad (2.3)$$

$$\mathbf{G} = -\frac{1}{2} \mathbf{CDC} \succeq 0 \quad (2.4)$$

The reverse of this property is also true, being that if $-\frac{1}{2} \mathbf{CDC} \succeq 0$, then \mathbf{D} is an EDM.

The EDM \mathbf{D} is unique up to rigid transformations: translation, reflection or rotation of the original set \mathbf{X} . However, this means that this orientation information is lost when constructing the EDM and cannot be recovered during MDS in Sec. 2.2.

Information regarding k (dimension of the original points in \mathbf{X}) is also lost when taking the L^2 norm, however this should not be a problem since in most practical applications this will be known beforehand or can be assumed to be 2- or 3-dimensional, since it will be used to reconstruct physical objects that are at most 3-dimensional.

2.2. Multidimensional Scaling

Multidimensional scaling (MDS), first proposed in 1952 by W.C. Torgerson [5] and also known as principal coordinates analysis (PCoA), is an algorithm that maps a set of points to an x -dimensional space so that their between-point distances are preserved as much as

possible with a given EDM. Stated simply, MDS translates an EDM back into a set of points of arbitrary dimension.

This algorithm, as outlined in *An Introduction to MDS* [6], is given in Al. 2.1.

Algorithm 2.1: Classical MDS

Require: EDM \mathbf{D} of size $n \times n$

Require: k as required dimensions of map

$\mathbf{C} \leftarrow \mathbf{I}_n - \frac{1}{n}\mathbf{1}_n\mathbf{1}_n^\top$	▷ Get centering matrix
$\mathbf{G} \leftarrow -\frac{1}{2}\mathbf{CDC}$	▷ Get Gram matrix
$\mathbf{U}, \{\lambda_{1\dots n}\} \leftarrow \text{EVD}(\mathbf{G})$	▷ Eigenvalue decomposition of Gram matrix
$\mathbf{\Lambda}_k \leftarrow \text{diag}(\lambda_1, \lambda_2 \dots \lambda_k)$	▷ Get diagonal matrix with k largest eigenvalues
$\mathbf{U}_k \leftarrow (U_1 U_2 \dots U_k)$	▷ Concatenate k largest eigenvectors
$\hat{\mathbf{X}} \leftarrow \mathbf{U}_k \sqrt{\mathbf{\Lambda}_k}$	▷ Get projected points
return $\hat{\mathbf{X}}$	

The matrix $\hat{\mathbf{X}}$ returned by this algorithm is the matrix that minimizes the loss function known as 'Stress', given below [7]:

$$\text{Stress}_{\mathbf{D}}(\hat{\mathbf{x}}_1, \hat{\mathbf{x}}_2, \dots, \hat{\mathbf{x}}_n) = \sqrt{\sum_{i \neq j=1 \dots n} (\mathbf{D}_{ij} - \|\hat{\mathbf{x}}_i - \hat{\mathbf{x}}_j\|_2^2)^2} \quad (2.5)$$

This loss function can be interpreted as Root Mean Squared Error (RMSE) of the differences between the original and reconstructed EDM. Since the algorithm discards all but the largest eigenvalues, it is concluded that MDS is relatively robust to Gaussian noise in the EDM. This property is also attested in a paper by Peterfreund and Gavish [8].

While MDS is very efficient when working with full EDM's (distance between every point and every other point is known), in practice this is an almost impossible requirement.

In the first case, the number of distances that must be known (read: measured) can be stated as a k -combinations problem with n as the number of points in the system.

$$\binom{n}{2} = \frac{n!}{2!(n-2)!} = \frac{1}{2}(n)(n-1) = \frac{1}{2}n^2 - \frac{1}{2}n \quad \therefore O(n^2) \quad (2.6)$$

Stated otherwise, the number of measurements needed to fully define the EDM of a system of points increases with quadratic order, making it intractable for large systems.

Secondly, it is not always possible to measure the distance between every pair of points in the system, e.g. if one point is visible from one perspective but not another, leading to gaps in the EDM. The EDM has no mechanism to flag which of these measurements are missing (crucially, a value of 0 would imply that the points have no distance between them). Naively discarding every point that is not fully connected to every other also discards valid measurements that contain valuable information that could be used during reconstruction and may reduce the MDS's ability to fully capture the shape being reconstructed.

In the next section, semidefinite programming (SDP) will be used to transform a semi-defined EDM into a fully defined EDM that can be used by the MDS algorithm.

2.3. Semidefinite Programming

Seemingly a misnomer, semidefinite programming (SDP), is a type of optimisation that minimizes a user defined loss function over the intersection of positive semidefinite matrices and an affine space. In other words, SDP finds a positive semidefinite matrix that both minimizes error as defined by the user and is an element of a given space.

In this section, SDP will be used to fill a fully defined EDM $\hat{\mathbf{D}}$ from a semi-defined EDM $\tilde{\mathbf{D}}$. As mentioned previously in Sec. 2.2, An EDM has no intrinsic way of flagging missing distance measurements, since a value of zero would imply that the two points defined by that entry must lie at the same position. This problem is addressed by defining a mask matrix \mathbf{W} from an index set of valid measurements \mathcal{E} (where a value of 1 at w_{ij} would indicate that a measurement exists between \mathbf{x}_i and \mathbf{x}_j in the original set \mathbf{X}):

$$w_{ij} \stackrel{\text{def}}{=} \begin{cases} 1 & (i, j) \in \mathcal{E} \\ 0 & \text{otherwise} \end{cases} \quad (2.7)$$

Recall from Eq. 2.4 that for an EDM \mathbf{D} , its Gram matrix \mathbf{G} is positive semidefinite while also being geometrically centered. Therefore, there is a direct map from the space of possible EDM's (\mathbb{EDM}^n) to the intersection of possible positive semidefinite matrices \mathbb{R}_+^n and symmetric, geometrically centered matrices \mathbb{S}_c^n . Using this correspondence, the problem can be used to cast EDM completion as a relaxed semidefinite program [9]:

$$\underset{\mathbf{G}}{\text{minimize}} \quad \|\mathbf{W} \circ (\tilde{\mathbf{D}} - \mathcal{K}(\mathbf{G}))\|_F^2 \quad (2.8)$$

$$\text{subject to} \quad \mathbf{G} \in \mathbb{R}_+^n \cap \mathbb{S}_c^n \quad (2.9)$$

Also from [9], the constraint $\mathbf{G} \in \mathbb{S}_c^n$ implies that \mathbf{G} has a nullspace (at least one of its eigenvalues must be 0) that may cause numerical problems. To solve this, some sort of invertible transformation must be applied to \mathbf{G} to transform it to a lower dimensional space, removing the part responsible for the nullspace. Dokmanić *et al.* proposes the following transformation:

$$\mathcal{G}_{n-1}(\mathbf{D}) \stackrel{\text{def}}{=} -\frac{1}{2}\mathbf{V}^\top \mathbf{D} \mathbf{V} \quad \text{where} \quad \mathcal{G}_{n-1}(\mathbf{D}) \in \mathbb{R}_+^{n-1} \quad (2.10)$$

$$\mathbf{V} = \begin{bmatrix} p & p & \dots & p \\ 1+q & q & \dots & q \\ q & 1+q & \dots & q \\ \vdots & \vdots & \ddots & \vdots \\ q & q & \dots & 1+q \end{bmatrix} \quad \text{such that } \mathbf{V} \in \mathbb{R}_+^{n \times (n-1)} \quad \text{and} \quad \mathbf{V}^\top \mathbf{V} = 1 \quad (2.11)$$

$$\therefore p = -\frac{1}{n + \sqrt{n}} \quad \text{and} \quad q = -\frac{1}{\sqrt{n}} \quad (2.12)$$

Additionally:

$$\mathcal{K}(\mathbf{V}\mathcal{G}_{n-1}(\mathbf{D})\mathbf{V}^\top) = \mathbf{D} \quad (2.13)$$

Therefore, $\mathbf{H} \mapsto \mathcal{K}(\mathbf{V}\mathbf{H}\mathbf{V}^\top)$ is an invertible map from \mathbb{R}_+^{n-1} to \mathbb{EDM}^n . Using this observation, a more numerically stable SDP can be constructed:

$$\underset{\mathbf{H}}{\text{minimise}} \quad \left\| \mathbf{W} \circ (\tilde{\mathbf{D}} - \mathcal{K}(\mathbf{V}\mathbf{H}\mathbf{V}^\top)) \right\|_F^2 \quad (2.14)$$

$$\text{subject to } \mathbf{H} \in \mathbb{R}_+^{n-1} \quad (2.15)$$

However, as mentioned by Krislock & Wolkowicz [10], this solution allows movement of the points in higher dimensions even if there is a valid solution in k -dimensions. A heuristic for promoting lower dimensions can be found by maximising the trace of the Gram matrix, as proposed by Biswas, *et al.* [11]. This stretches out the points as much as possible, favouring smaller, affine dimensions (as if smoothing out a crumpled piece of paper). Finally, noting that $\text{tr}(\mathbf{G}) = \text{tr}(\mathbf{H})$, the SDP can be rewritten [9], including the data fidelity term proposed by Biswas, *et al.*¹:

$$\underset{\mathbf{H}}{\text{maximise}} \quad \text{tr}(\mathbf{H}) - \lambda \left\| \mathbf{W} \circ (\tilde{\mathbf{D}} - \mathcal{K}(\mathbf{V}\mathbf{H}\mathbf{V}^\top)) \right\|_F^2 \quad (2.16)$$

$$\text{subject to } \mathbf{H} \in \mathbb{R}_+^{n-1} \quad (2.17)$$

A Matlab/CVX [12] [13] script of this SDP can be found in App. C. Once this matrix \mathbf{H} is determined, the approximate EDM $\hat{\mathbf{D}}$ can be determined:

$$\hat{\mathbf{D}} = \mathcal{K}(\mathbf{V}\mathbf{H}\mathbf{V}^\top) \quad (2.18)$$

This EDM $\hat{\mathbf{D}}$ is guaranteed to be fully defined and can then be used by the MDS of Sec. 2.2 to create a reconstruction $\hat{\mathbf{X}}$.

¹This value for λ is determined to be 10 experimentally in Sec. 5.2

2.4. Rotation Matrix Estimation

As mentioned in Sec. 2.1, the EDM loses information regarding the orientation and dimension of \mathbf{X} . While the dimension k of the reconstructed points $\hat{\mathbf{X}}$ can usually be inferred by the implementation (e.g. 3-dimensional when working with stereo cameras), the lost information allows a reconstruction that is accurate only up to translation, rotation and reflection. If the points \mathbf{X} or a subset thereof are known, a transformation can be applied to $\hat{\mathbf{X}}$ to align it with \mathbf{X} . The next sections will illustrate this transformation.

2.4.1. Naive Inverse Matrix

If the true values are known, the naive solution would be to construct a transformation matrix that could be applied to $\hat{\mathbf{X}}$ to rotate it to the same orientation as \mathbf{X} . Firstly, taking the first points, \mathbf{x}_1 and $\hat{\mathbf{x}}_1$, arbitrarily as the origin of the new coordinate system, \mathbf{X} and $\hat{\mathbf{X}}$ are translated to align with this assumption by broadcasting this subtraction to all of the points in the set:

$$\mathbf{X}_t = \mathbf{X} - \mathbf{1}_n \mathbf{x}_1 \quad \text{where } \mathbf{X} \in \mathbb{R}^{n \times k} \quad \text{and } \mathbf{x}_1 \in \mathbb{R}^{1 \times k} \quad (2.19)$$

$$\hat{\mathbf{X}}_t = \hat{\mathbf{X}} - \mathbf{1}_n \hat{\mathbf{x}}_1 \quad \text{where } \hat{\mathbf{X}} \in \mathbb{R}^{n \times k} \quad \text{and } \hat{\mathbf{x}}_1 \in \mathbb{R}^{1 \times k} \quad (2.20)$$

The transformation matrix \mathbf{T} is calculated using the inverse of \mathbf{X}_t below:

$$\hat{\mathbf{X}}_t \mathbf{T} = \mathbf{X}_t \quad (2.21)$$

$$\hat{\mathbf{X}}_t^{-1} \hat{\mathbf{X}}_t \mathbf{T} = \hat{\mathbf{X}}_t^{-1} \mathbf{X}_t \quad (2.22)$$

$$\mathbf{T} = \hat{\mathbf{X}}_t^{-1} \mathbf{X}_t \quad (2.23)$$

With the transformation matrix \mathbf{T} , it is applied to $\hat{\mathbf{X}}_t$ to obtain the rotated set of points:

$$\hat{\mathbf{X}}_t \mathbf{T} = \hat{\mathbf{X}}_{\text{rot}} \quad (2.24)$$

However, since $\hat{\mathbf{X}}_t$ is non-square ($\hat{\mathbf{X}}_t \in \mathbb{R}^{n \times d}$) it is not invertible and singular. This problem is addressed in the next section.

2.4.2. Moore-Penrose Inverse Matrix

While $\hat{\mathbf{X}}_t$ does not have an inverse, the Moore-Penrose inverse $\hat{\mathbf{X}}_t^+$ can be calculated that corresponds to a least squares solution of the system of linear equations represented by $\hat{\mathbf{X}}_t$. This matrix is a left inverse ($\hat{\mathbf{X}}_t^+ \hat{\mathbf{X}}_t = \mathbf{I}$) when $\text{rank}(\hat{\mathbf{X}}) \geq k$ (columns are linearly independent) allowing its use in same fashion as above.

$$\mathbf{X}_t = \mathbf{X} - \mathbf{1}_n \mathbf{x}_1 \quad \text{where } \mathbf{X} \in \mathbb{R}^{n \times k} \quad \text{and } \mathbf{x}_1 \in \mathbb{R}^{1 \times k} \quad (2.25)$$

$$\hat{\mathbf{X}}_t = \hat{\mathbf{X}} - \mathbf{1}_n \hat{\mathbf{x}}_1 \quad \text{where } \hat{\mathbf{X}} \in \mathbb{R}^{n \times k} \quad \text{and } \hat{\mathbf{x}}_1 \in \mathbb{R}^{1 \times k} \quad (2.26)$$

$$\hat{\mathbf{X}}_t \mathbf{T} = \mathbf{X}_t \quad (2.27)$$

$$\hat{\mathbf{X}}_t^+ \hat{\mathbf{X}}_t \mathbf{T} = \hat{\mathbf{X}}_t^+ \mathbf{X}_t \quad (2.28)$$

$$\mathbf{T} = \hat{\mathbf{X}}_t^+ \mathbf{X}_t \quad (2.29)$$

As before this transformation matrix is applied to $\hat{\mathbf{X}}_t$ to rotate the set of points:

$$\hat{\mathbf{X}}_t \mathbf{T} = \hat{\mathbf{X}}_{\text{rot}} \quad (2.30)$$

While certainly powerful and simple, this transformation is critically not distance preserving since $\det(\mathbf{T})$ is not guaranteed to equal 1, leading to possible distortions when applied to the set of reconstructed points.

2.4.3. Kabsch Algorithm and Householder Matrix

A solution to the distortion problem of the Moore-Penrose Inverse would be to use the Kabsch algorithm [14], also known as a constrained orthogonal Procrustes problem subject to a unitary transformation. This algorithm returns the optimal rotation matrix that minimizes the RMSE between all or a subset of \mathbf{X} and the transformed corresponding $\hat{\mathbf{X}}$.

This rotation matrix obtained with the Kabsch algorithm is also guaranteed to have a determinant of 1, meaning that there is no distortion when applied to the EDM.

Recall that the reconstruction is only accurate up to translation, rotation and reflection. Crucially, reflection. Since the Kabsch algorithm only returns a rotation matrix, the "handedness" of the reconstruction $\hat{\mathbf{X}}$ must be corrected to conform to the true, known set \mathbf{X} . This requires a subset (\mathbf{X}_{sub} and their reconstructed points $\hat{\mathbf{X}}_{\text{sub}}$) of at least 3 known point pairs other than \mathbf{x}_1 and $\hat{\mathbf{x}}_1$, which is assumed to be the origin of the shared coordinate systems. As before, \mathbf{x}_1 and $\hat{\mathbf{x}}_1$ are first used to align \mathbf{X} and $\hat{\mathbf{X}}$ (and by extension,

their subsets) with this assumption:

$$\mathbf{X}_t = \mathbf{X} - \mathbf{1}_n \mathbf{x}_1 \quad \text{where } \mathbf{X} \in \mathbb{R}^{n \times k} \quad \text{and } \mathbf{x}_1 \in \mathbb{R}^{1 \times k} \quad (2.31)$$

$$\hat{\mathbf{X}}_t = \hat{\mathbf{X}} - \mathbf{1}_n \hat{\mathbf{x}}_1 \quad \text{where } \hat{\mathbf{X}} \in \mathbb{R}^{n \times k} \quad \text{and } \hat{\mathbf{x}}_1 \in \mathbb{R}^{1 \times k} \quad (2.32)$$

Next, the normal unit vector to the plane defined by the first two points in the subsets is determined:

$$\hat{\mathbf{v}} = \left\| \hat{\mathbf{x}}_{\text{sub}_1} \times \hat{\mathbf{x}}_{\text{sub}_2} \right\|_2 \quad (2.33)$$

$$\mathbf{v} = \left\| \mathbf{x}_{\text{sub}_1} \times \mathbf{x}_{\text{sub}_2} \right\|_2 \quad (2.34)$$

Finally, the signs of the dot products between these normal unit vectors and the third point in the respective subsets is compared:

$$\text{sgn}(\mathbf{v} \cdot \left\| \mathbf{x}_{\text{sub}_3} \right\|_2) \stackrel{?}{=} \text{sgn}(\hat{\mathbf{v}} \cdot \left\| \hat{\mathbf{x}}_{\text{sub}_3} \right\|_2) \quad (2.35)$$

If the signs are equal, it can be concluded that the "handedness" of the systems are congruent and a rotation matrix can be determined directly using the Kabsch algorithm (by taking \mathbf{P} as \mathbf{I}_3 in Eq. 2.36). If the "handedness" differs, the subset $\hat{\mathbf{x}}_{\text{sub}}$ must be reflected across the plane defined by the normal unit vector $\hat{\mathbf{v}}$. To do this, the Householder matrix [15] \mathbf{P} is defined and applied to the subset and reconstructed set:

$$\mathbf{P} = \mathbf{I}_3 - 2\hat{\mathbf{v}}^\top \hat{\mathbf{v}} \quad (2.36)$$

$$\hat{\mathbf{X}}_{\text{refl}_{\text{sub}}} = \hat{\mathbf{X}}_{\text{sub}} \mathbf{P} \quad (2.37)$$

$$\hat{\mathbf{X}}_{\text{refl}} = \hat{\mathbf{X}}_t \mathbf{P} \quad (2.38)$$

This Householder matrix has the useful property of being guaranteed to have a determinant of -1 , meaning that no distortion of the EDM will occur, only a reflection of the points.

Once the handedness is confirmed, the Kabch algorithm can be applied:

$$\mathbf{H} = \hat{\mathbf{X}}_{\text{refl}_{\text{sub}}}^\top \mathbf{X}_{\text{sub}} \quad (2.39)$$

Taking the singular value decomposition (SVD) of \mathbf{H} (which can be seen as a cross-covariance matrix of $\hat{\mathbf{X}}_{\text{refl}_{\text{sub}}}^\top$ and \mathbf{X}_{sub}):

$$\mathbf{H} = \mathbf{U} \Sigma \mathbf{V}^\top \quad (2.40)$$

The rotation matrix is then calculated:

$$\mathbf{T} = \mathbf{V}\mathbf{U}^\top \quad (2.41)$$

Finally, this rotation matrix \mathbf{T} is applied to $\hat{\mathbf{X}}_t$ to rotate the set of points:

$$\hat{\mathbf{X}}_t \mathbf{T} = \hat{\mathbf{X}}_{\text{rot}} \quad (2.42)$$

The Kabsch algorithm alongside the Householder matrix has the advantage of needing only 4 known points to work, while additional points increase the accuracy of the rotation matrix obtained. This algorithm is also guaranteed to introduce no distortions in the reconstructed points since the resultant transformation is unitary:

$$|\det(\mathbf{T}) \cdot \det(\mathbf{P})| = 1 \quad (2.43)$$

2.5. Summary

This chapter has given the theoretical background required for the software implementation (Sec. 5.2) of the deterministic reconstruction algorithm of this report.

The foundation of this algorithm is that of the Euclidean distance matrix (EDM) of Sec. 2.1, a matrix describing the inter-point distances of the points to be reconstructed. With the EDM as a lynch-pin, the deterministic reconstruction algorithm can be viewed as a nested optimisation problem: multidimensional scaling (MDS, Sec. 2.2) optimises the resultant points of the reconstruction in 3-dimensional space subject to the constraint of the EDM of these points. In the case of a partially defined EDM (some distances between the points are not in the measurement set), this EDM is itself optimised with semidefinite programming (SDP, Sec. 2.3) subject to the constraint of the available, observed distances.

Due to orientation information not being encoded in the EDM, the resultant reconstruction is only up to translation, reflection and rotation. To reorient the reconstruction, three points that are not co-planar are used in conjunction with the Householder matrix and Kabsch algorithm (2.4.3) to obtain a rotation matrix that does not distort the reconstruction.

The next chapter will give the fundamental theory of the alternative to the deterministic algorithm, based on probability and inference.

Chapter 3

Probabilistic Reconstruction Methods

“The way to control and direct a Mentat, Nefud, is through his information. False information—false results.”

— Baron Harkonnen, *Dune* [16]

In contrast to the deterministic methods of Ch. 2, this chapter provides an alternative probabilistic solution to the reconstruction problem. This method has the advantage of using potential prior information effectively and being a simpler method to implement with less moving parts, ergo fewer sources of error.

This chapter introduces the probabilistic graphical model (PGM), a way to represent the belief of the system concerning the locations of the reconstructed points and how belief propagates across this network.

Using this model, along with prior distributions describing known positional knowledge and the unscented transform (UT) to “couple” the positional distributions based on the observed distance between them, the beliefs regarding the positions of the reconstructed points converge to values that are then returned.

A flowchart describing this method is given below:

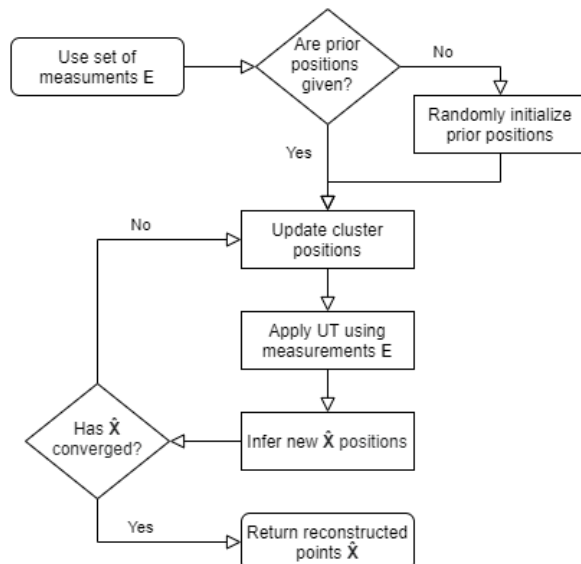


Figure 3.1: Probabilistic Reconstruction Method Flowchart

3.1. Probabilistic Graphical Model

Graphs, in the context of graph theory, are defined as a set of points (also called nodes or vertices) where in which some pairs of these points are connected by edges [17]. Edges may also be directed (i.e. edge has an orientation, e.g. from point a to point b) or undirected (i.e. edge orientation is irrelevant). A graph consisting of only directed edges is therefore known as a directed graph and, conversely, a graph with only undirected edges is known as undirected.

Probabilistic graphical models (PGM) are a specific subset of these graphs where the nodes of the graph represent dependencies/independencies in probability (or more general) distributions of random variables, showing how these random variables influence each other [18, p. 58].

3.1.1. Bayes and Markov Networks

Directed acyclic graphs (DAG) with nodes that are defined with conditional probability distributions (CPD) are known as Bayes Networks. These CPDs that define the graph G must satisfy the form $P(X | \text{Pa}_X^G)$, stating that the conditional probability of a random variable can only be conditional on the direct parents of that node. An example can be seen in Fig. 3.2a and its factorization in Eq. 3.2.

These Bayes networks model causal influence between its nodes very intuitively and show the causal flow of influence along its directed edges.

Bayes networks, however, cannot capture the mechanics of all systems, such in the famous XOR case [19, p. 82].

To solve this problem, a more general definition of the Bayesian network is used, that of the Markov random field (MRF) or Markov network. These networks can be cyclical, do not have directed edges and use a more general definition of distributions (that need not be CPDs) called factors. These factors map the random variables over which they are defined (the scope of the factor) to values, normally constrained to be positive.

An example of a factor, $\phi(A, B)$, for $A, B \in \{0, 1\}$ is given by:

$$\phi(A, B) = \begin{array}{cc|c} A^0 & B^0 & 1 \\ A^0 & B^1 & 0 \\ A^1 & B^0 & 5 \\ A^1 & B^1 & 1000 \end{array} \quad (3.1)$$

It is important to note is the fact that these factors do not have to sum to 1, since they do not necessarily have to be probability distributions. Therefore, to convert the product of the factors that factorize a MRF (known as an unnormalized measure) to a valid, joint probability distribution, a normalizing factor of $\frac{1}{Z}$ must be added to this product, where

Z is known as the partition function, as seen in Eq. 3.3.

These two graph types can be converted to the other through a process known as moralisation¹. This is visually shown by the two equivalent graphs of Fig. 3.2:

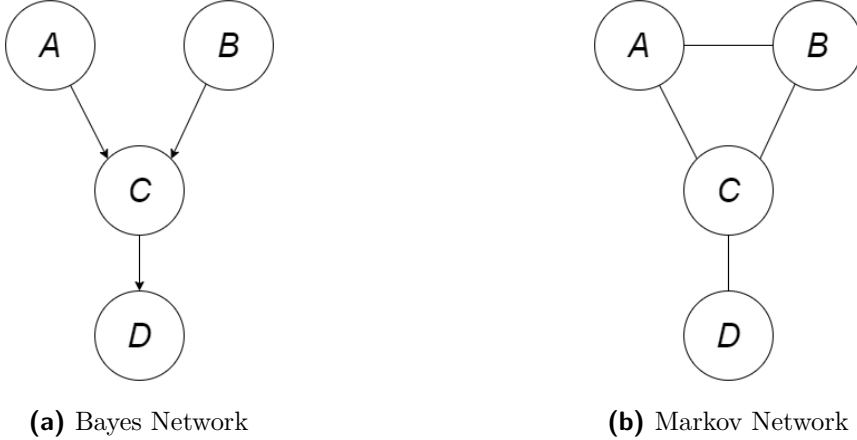


Figure 3.2: Equivalent Bayes and Markov Networks

The Bayes network in Fig. 3.2a is defined by the equation:

$$P(A, B, C, D) = P(A)P(B)P(C | A, B)P(D | C) \quad (3.2)$$

And its Markov network equivalent (obtained through moralisation) in Fig. 3.2b is defined by the equation:

$$\begin{aligned} P(A, B, C, D) &= \frac{1}{Z} \phi(A, B, C) \phi(C, D) \\ \text{with } Z &= \sum_{A,B,C,D} \phi(A, B, C) \phi(C, D) \end{aligned} \quad (3.3)$$

For the application of reconstruction, taking the positional coordinates of the reconstructed points as random variables, an undirected MRF model is more fitting. Since distance is bidirectional, a Bayes network with directed edges would be extremely cyclical to account for this bidirectional flow of positional information between the points.

An additional problem arises from taking the positional coordinates of the reconstructed points as random variables, since these coordinates are not discrete. Therefore, the next section will detail the continuous extension of the MRF using Gaussian distributions.

As an additional note, while it is certainly possible to discretise the coordinate space for the positional random variables, to do so for any acceptable level of accuracy would be prohibitively computationally expensive given the fact that the size of a factor grows quadratically with the possible values that its random variables can take.

¹A humorous convention, since the direct parents of a node become connected, a pseudo-”moral” thing to do.

An additional, although relative, benefit of using continuous factors is that the computational complexity to describe the network parameters drops from exponential ($O(2^n)$) to cubic ($O(n^3)$) complexity.

3.1.2. Gaussian Markov Random Fields

As mentioned previously in Sec. 3.1.1, the space of parameterisations for representing a continuous variable with discrete factors is essentially unbounded [19, p. 247].

This subsection details the extension of the Markov Random Field (MRF) to the continuous case using the alternate representation of multivariate Gaussian distributions, the information form.

The standard form of representing a multivariate distribution with a mean vector μ and a $n \times n$ covariance matrix Σ is given by the following equation:

$$p(\mathbf{x}) = \frac{1}{\sqrt{(2\pi)^n |\Sigma|}} \exp \left[-\frac{1}{2} (\mathbf{x} - \boldsymbol{\mu})^\top \Sigma^{-1} (\mathbf{x} - \boldsymbol{\mu}) \right] \quad (3.4)$$

Considering the exponent in Eq. 3.4 and taking the inverse of the covariance matrix as \mathbf{J} (known as the precision or information matrix), the exponent can be rewritten:

$$-\frac{1}{2} (\mathbf{x} - \boldsymbol{\mu})^\top \mathbf{J} (\mathbf{x} - \boldsymbol{\mu}) = -\frac{1}{2} (\mathbf{x}^\top \mathbf{J} \mathbf{x} - 2\mathbf{x}^\top \mathbf{J} \boldsymbol{\mu} + \boldsymbol{\mu}^\top \mathbf{J} \boldsymbol{\mu}) \quad (3.5)$$

Noting that the last term is a constant:

$$p(\mathbf{x}) \propto \exp \left[-\frac{1}{2} \mathbf{x}^\top \mathbf{J} \mathbf{x} + (\mathbf{J} \boldsymbol{\mu})^\top \mathbf{x} \right] \quad (3.6)$$

This alternate representation is known as the information form, with $\mathbf{h} = \mathbf{J} \boldsymbol{\mu}$ known as the potential vector [19, p. 248].

The advantage of this form is that independence between variables can be read directly from the information matrix. This can be seen below in Th. 7.2 from Koller [19, p. 251].

Koller Theorem 7.2. *Consider a Gaussian distribution $p(X_1, \dots, X_n) = \mathcal{N}(\boldsymbol{\mu}, \Sigma)$, and let $\mathbf{J} = \Sigma^{-1}$ be the information matrix. Then $\mathbf{J}_{i,j} = 0$ if and only if $p \models (X_i \perp X_j \mid \mathcal{X} - \{X_i, X_j\})$*

Since that the information matrix can be used to describe the independencies in a set of continuous variables, the information matrix can now be used to capture the independencies of a Markov network (the nodes that are not connected).

Therefore, using this theorem, any Markov network of continuous variables can be represented by a multivariate Gaussian in the information form.

3.2. Unscented Transform

Introduced as part of the unscented Kalman filter (UKF)² by Julier and Uhlmann [20], the unscented transform approximates a non-linear transformation of a Gaussian distribution through deterministic sampling of a minimal set of sample points (known as sigma points) transformed by a non-linear function which is used to estimate a new mean and covariance of the transformed Gaussian.

From [20], the Unscented Transform of the d -dimensional random variable \mathbf{X} with mean vector $\boldsymbol{\mu}$ and covariance matrix $\boldsymbol{\Sigma}$ can be described by $2d + 1$ weighted points \mathcal{X} :

$$\mathcal{X}_0 = \boldsymbol{\mu} \quad W_0 = \frac{\kappa}{d + \kappa} \quad (3.7)$$

$$\mathcal{X}_i = \boldsymbol{\mu} + \left(\sqrt{(d + \kappa)\boldsymbol{\Sigma}} \right)_i \quad W_i = \frac{\kappa}{2(d + \kappa)} \quad (3.8)$$

$$\mathcal{X}_{i+d} = \boldsymbol{\mu} - \left(\sqrt{(d + \kappa)\boldsymbol{\Sigma}} \right)_i \quad W_{i+d} = \frac{\kappa}{2(d + \kappa)} \quad (3.9)$$

where $\mathcal{X} \in \mathbb{R}^{d \times (2d+1)}$ and $\kappa \in \mathbb{R}$

W_i indicates the weight of the i th point and $\left(\sqrt{(d + \kappa)\boldsymbol{\Sigma}} \right)_i$ denotes the i th row or column of the matrix square root \mathbf{L} obtained using the Cholesky decomposition:

$$\left(\sqrt{(d + \kappa)\boldsymbol{\Sigma}} \right) = \mathbf{L}\mathbf{L}^\top \quad (3.10)$$

These points can then be transformed using a potentially non-linear function:

$$\mathcal{Y}_i = f(\mathcal{X}_i) \quad (3.11)$$

The approximated new mean is given by the weighted average of the transformed points and the approximated new covariance matrix is given by the weighted outer product of the transformed points:

$$\tilde{\boldsymbol{\mu}} = \sum_{i=0}^{2d} W_i \mathcal{Y}_i \quad (3.12)$$

$$\tilde{\boldsymbol{\Sigma}} = \sum_{i=0}^{2d} W_i (\mathcal{Y}_i - \tilde{\boldsymbol{\mu}})(\mathcal{Y}_i - \tilde{\boldsymbol{\mu}})^\top \quad (3.13)$$

This approximated mean and covariance is then used to construct the new Gaussian

²The apocryphal origin of this name is purported to either be Uhlmann not wanting the UKF to be named after himself or that the UKF was named in response to the "rotten"[sic] extended Kalman filter, although no extensive academic research has been done to ascertain the veracity of these claims.

distribution for the transformed random variable \mathbf{Y} :

$$\mathbf{Y} \sim \mathcal{N}(\tilde{\boldsymbol{\mu}}, \tilde{\boldsymbol{\Sigma}}) \quad (3.14)$$

Eq. 3.11 can also be used to increase the dimension of the original Gaussian. By observing this additional axis, the original distribution can be shifted according to Eq. 3.11.

This hyperplane created by observing the additional axis is demonstrated in the reduced dimensional example in Fig. 3.3 below. In this example, the random variable x , represented by a zero-mean Gaussian, gains an additional dimension y using the unscented transform given by the following simple linear transform:

$$y = x - 4 \quad (3.15)$$

Observing values for y creates the hyperplanes that intersect the transformed multivariate Gaussian as seen in Fig. 3.3. By inspecting the means of the new Gaussians defined in x , it is clear that the values of the new means are roughly 4 more than the observed values, as expected from Eq. 3.15.

Figure 3.3: Simplified Hyperplane Example³. Observe how the mean of the Gaussian intersection shifts in time with the movement of the hyperplane.

For the application of reconstruction, this transform is used to "couple" two three-dimensional Gaussians (the prior coordinates of the points) by adding an additional

³Requires Adobe Acrobat or Okular PDF viewer to display animation.

dimension that is a non-linear function (Euclidean distance between the points) of the other six positional dimensions:

$$\mathbf{Y} = f(\mathbf{X}) \quad (3.16)$$

$$\text{where } \mathbf{X} = \begin{bmatrix} x_1 \\ \vdots \\ x_6 \end{bmatrix} \quad \text{and} \quad \mathbf{Y} = \begin{bmatrix} x_1 \\ \vdots \\ x_6 \\ d \end{bmatrix} \quad \text{and} \quad d = \sqrt{(x_1 - x_4)^2 + (x_2 - x_5)^2 + (x_3 - x_6)^2}$$

By observing the distance d value of \mathbf{Y} , a hyperplane through the seven-dimensional distribution is taken that relates the two constituent three-dimensional distributions according to their measured distance.

This can be observed in the simplified 2-dimensional case given by Fig. 3.4, where the two initial 1-dimensional Gaussians have a distance of 10 between their means. However, after applying the unscented transform as in Eq. 3.16 and observing the distance on the added axis to be 3, these distributions are shifted to conform to this observation.

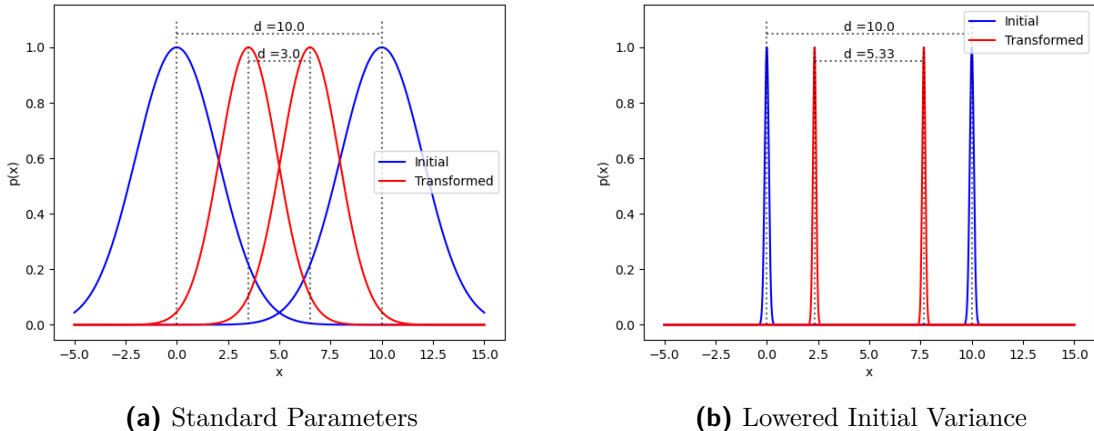


Figure 3.4: Simplified Unscented Transform with Observed Distance Example

When looking at Fig. 3.4b, it is enlightening to note, however, that this process may struggle when the locations of the initial distributions are well defined (i.e. low variance). In a sense, the system is already certain of the distance between the points and is very resistant to change this belief. This process also reduces the variance of the points at each step, potentially causing numerical issues, such as underflow, after repeated applications and must be considered during implementation.

3.3. Positional Inference

At each iteration of the loop for the probabilistic reconstruction algorithm, after the prior positions have been readjusted using the observed distances alongside the UT, known positions have been observed and the new positional beliefs have been propagated across the network, new positional distributions must be inferred to serve as priors for the next iteration.

By saving a copy of these inferred positions, inferred positions of the next loop of the probabilistic algorithm (implemented in Sec. 5.3), can be compared against until a certain tolerance of convergence is reached.

3.3.1. Marginal Inference

As seen in Eq. 3.3, a Markov Network can be represented as a joint probability distribution by taking the normalized product of its factors.

Marginal inference is a simple method of inference that computes the distribution of a subset of variables from the distribution that is possibly conditioned on a set of evidence [18, p. 77].

As an example, consider the joint probability distribution of the discrete random variables $P(x_1, x_2, x_3, x_4)$ and the observed evidence $x_4 = 2$. For the distribution of $p(x_1)$:

$$P(x_1 | x_4 = 2) = \sum_{x_2, x_3} P(x_1, x_2, x_3, x_4 = 2) \quad (3.17)$$

Applying this to the case of reconstruction, assuming that every point in a set of n points is described by three random continuous variables ($\mathcal{P}_i = \{p_{ix}, p_{iy}, p_{iz}\} \forall 1 \leq i \leq n$ from the set of all positional random variables \mathcal{P}), the marginal inference can repeatedly be applied to the joint distribution of all of the positional random variables conditioned on the subset of known positions (e.g. the set $\mathcal{O} = \{p_{j_x} = x_{j_{\text{obs}}}, \dots, p_{k_z} = z_{k_{\text{obs}}}\}$ where $j, k \in [1, 2, \dots, n]$):

$$P(p_{ix} | \mathcal{O}) = \int_{-\infty}^{\infty} \int_{-\infty}^{\infty} \dots \int_{-\infty}^{\infty} P(p_{1x}, p_{1y}, p_{1z}, \dots, p_{nx}, p_{ny}, p_{nz}, \mathcal{O}) dp_{1x} dp_{1y} \dots dp_{nz} \quad (3.18)$$

From these distributions for the positional random variables, the maximum a posteriori (MAP) estimate can be taken which, since these are Gaussian distributions, is the mean.

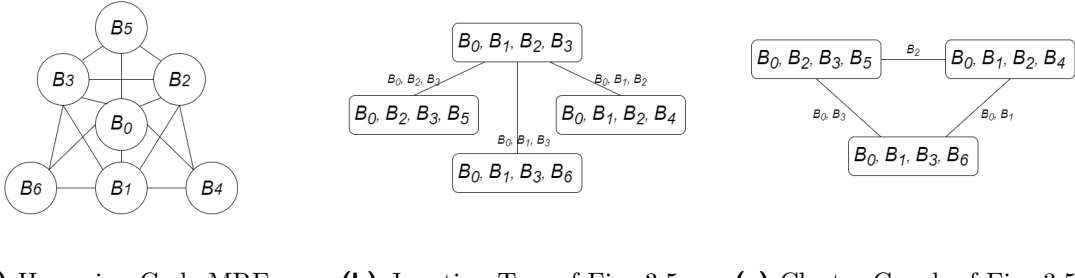
3.3.2. Junction Tree Algorithm

As shown in Sec. 3.1.1 and 3.3.1, propagating belief and inferring the values of the variables in a Markov network requires marginalising the full joint probability of all of the random variables in the network (obtained by taking the product of all of the factors as seen in

Eq. 3.3).

Calculating this joint probability, however, is computationally expensive and may be intractable for large systems.

A more efficient algorithm for the purpose of belief propagation is that of the junction tree algorithm. This algorithm constructs a new graph of connected subsets of the set of random variables ("clusters") that satisfies the running intersection property⁴ (RIP) and where every cluster is fully connected ("cliques"). Belief about variables shared between subsets ("sepset") is propagated using the message passing algorithm. A junction tree of Fig. 3.5a is given by Fig. 3.5b.



(a) Hamming Code MRF (b) Junction Tree of Fig. 3.5a (c) Cluster Graph of Fig. 3.5a

Figure 3.5: Junction Tree and Cluster Graph of 6-bit Hamming Code. Note that B_0 has been omitted from the uppermost sepset in Fig. 3.5c to preserve the RIP.

Fortunately, the size of the reconstruction problem in this report is small enough to simply use the joint distribution of all of the positional random variables⁵.

3.3.3. Loopy Belief Propagation

In the case of large networks or networks with high interconnectivity, it may be intractable to calculate a junction tree of Sec. 3.3.2 or the gains from doing so would be slim as the cliques would be very large. In these cases, alternative, approximate inference algorithms may be used such as loopy belief propagation.

This algorithm uses techniques similar to those in the junction tree algorithm (Sec. 3.3.2), notably message passing. The important distinction, however, is that while the junction tree (Fig. 3.5b) is guaranteed to be free of loops, the loopy belief propagation algorithm constructs a cluster graph (Fig. 3.5c) from directly from the factors while obeying the RIP. This differing construction creates the possibility of loops in the cluster tree, meaning that the inferred positions obtained using message passing is now iterative and approximate.

⁴For every variable, the subgraph formed by the clusters that contain that variable and the links between them, must form a tree.

⁵In some sense, the full joint is simply the simplest case of the junction tree algorithm, with the singular cluster being the full set of variables

3.4. Summary

This chapter has illustrated the essential concepts required for the implementation of the probabilistic algorithm (given in Sec. 5.3), the alternative to the deterministic algorithm of Ch. 2.

Firstly, Sec. 3.1 showed how belief networks can be constructed with probabilistic random variables that correspond to the positions of the reconstructed positions. Next, Sec. 3.2 introduced the unscented transform (UT), a function that adjusts the distributions of the positional random variables such that they conform to the observed distances from the measurement set. Finally, to infer the resultant positions, Sec. 3.3 gives various methods to obtain a value for each of the positional random variables (in the case of this report, the simplest method of marginal inference of the full joint distribution from Sec. 3.3.1 is used).

Due to the fact that the UT is an approximation, the results obtained from a single application of these methods is not exact. Therefore, the process is applied iteratively until the positional values converge (as seen in Sec. 5.3).

As opposed to the deterministic algorithm of Ch. 2, which views reconstruction as an optimisation problem, the probabilistic algorithm of this chapter uses a different paradigm, one of inference (logical deduction). Shifting from a constraint- to evidence-based approach has numerous advantages, chief among these being that fewer measurements are needed (since the problem does not have a minimum number of constraints) and that prior knowledge of the point positions can be incorporated. This approach of logical reasoning, however, does have the drawback that the system may not be as robust to measurement noise and record corruption, since system is more inclined to "believe" the faulty measurements as opposed to optimising these errors out.

The next chapter attempts to alleviate this potential drawback by proposing methods to identify and remove these faulty measurements, reducing the error of the reconstruction.

Chapter 4

Finding Erroneous Distance Measurements

Then, as his planet killed him, it occurred to Kynes that his father and all the other scientists were wrong, that the most persistent principles of the universe were accident and error.

— Liet Kynes, *Dune* [16]

Beside the expected measurement noise, in practice there may be distance records that are completely wrong, either measured between the wrong pair of points or the distance could be wildly incorrect. Whether due to human- or machine error, these errors must be identified and removed to improve reconstruction performance.

This chapter introduces a heuristic method in Sec. 4.1 for identifying these measurements based on the relative change between the original distance measurements and the distance measurements of the reconstructed points. A flowchart describing this method is given below in Fig. 4.1 below.

A possible improvement of this method is proposed in Sec. 4.2, which eschews the heuristic method for a probabilistic one. However, since the development of this method is outside the scope of this report, only the feasibility of this method is explored.

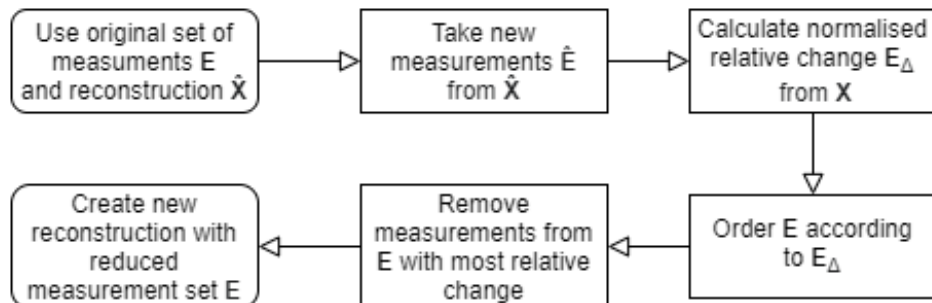


Figure 4.1: Heuristic Error Identification Method Flowchart

4.1. Heuristic Identification

The naive intuition used by this method is that the distances that change the most in the reconstruction versus the original distance measurement should be the ones that are anomalous. This feels logical, since if a point is described by ten distances from other points and one of these measurements are wrong, the point is "pulled" to the correct position against the influence of the incorrect measurement.

Therefore, ordering the distance measurements in the set \mathcal{E} by their normalized, relative change when compared to the corresponding distances in the reconstructed set $\hat{\mathcal{E}}$:

$$\mathcal{E}_\Delta = \frac{|\mathcal{E} - \hat{\mathcal{E}}|}{\mathcal{E}} \quad (4.1)$$

$$\mathcal{E}_{\text{ord}} = \text{sort}_{\text{asc}}(\mathcal{E} | \mathcal{E}_\Delta) \quad (4.2)$$

Now \mathcal{E}_{ord} represents the distance measurements used in the reconstruction that are in ascending order based on their relative change after reconstruction. From this, the last $x\%$ of measurements can be removed based on the error prevalence (err%) in the set. This reduced set of measurements are then used to reconstruct a new set of points with reduced reconstruction error.

This method can be used by both the deterministic- and probabilistic methods of Ch. 2 and 3, since it is only concerned with the original and reconstructed measurement sets (\mathcal{E} and $\hat{\mathcal{E}}$), not the method of reconstruction.

A limitation of this method is that the error prevalence percentage is something that must be known beforehand or determined experimentally during implementation.

It is also possible that measurements may be corrupted to values that are still somewhat valid, leading to situations where valid measurements that have been "pulled" by the presence of another anomalous measurement may score higher than these somewhat valid distances. In the worst case, these valid measurements may even be discarded by this heuristic, a situation that should obviously be avoided. This problem can be mitigated somewhat by only discarding a portion of the known error prevalence percentage (e.g. discard last $0.5 \times \text{err\%}$ elements of set \mathcal{E}_{ord}).

In a similar vein, this method may also struggle in the presence of noise, since *all* of the measurements will be distorted by the noise, making it harder to rank the measurements based on the relative change metric.

4.2. Probabilistic Identification

A possible improvement of the heuristic method of Sec. 4.1 is to solve the problem probabilistically. This has the advantage of identifying erroneous measurements based on

neighbouring measurements, avoiding the problems of falsely identifying distorted valid measurements and needing to know the global error prevalence percentage beforehand as encountered during the heuristic method.

Since this will most likely be a Gaussian-based solution, it should also be more robust to noise.

This method of identification is outside the scope of this report, however, and remains a tantalizing avenue of potential research.

4.3. Summary

This chapter has outlined two approaches to identifying corrupted records in the measurement set used by the reconstruction algorithms of Ch. 2 and 3.

The first of these methods is a heuristic algorithm that uses the normalised change between the original measurement and the corresponding measurement from the reconstruction as an indicator for flagging anomalous records. The implementation of this algorithm is given in Sec. 5.4 of the next chapter.

The second method is a probabilistic algorithm for identifying corrupted measurements by comparing each measurement to its local neighbours. If the measurement does not agree with the consensus of its neighbours, it is a good indication that the measurement is incorrect. The implementation of this algorithm is outside the scope of this report and only the outline of the algorithm is given.

The next chapter will review the implementation of the algorithms from Ch 2, 3 and this chapter, as well as the testing framework for evaluating the performance of these algorithms.

Chapter 5

Experimental Setup

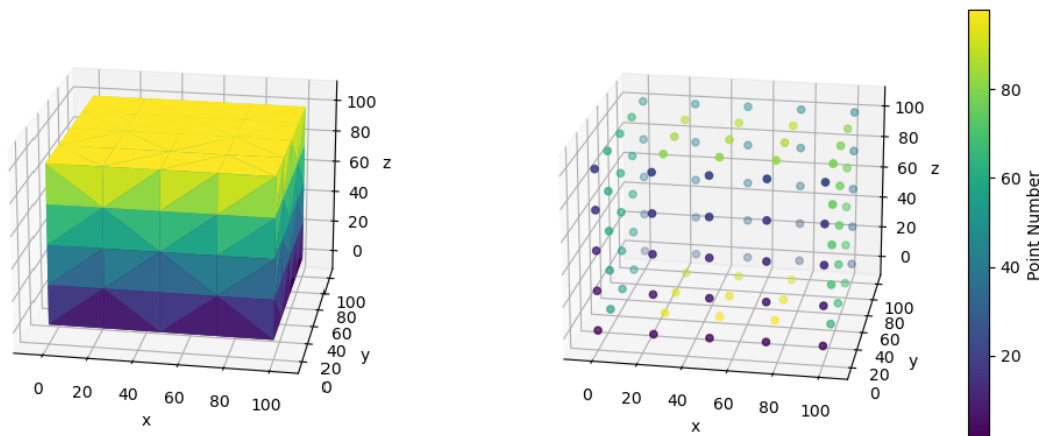
A beginning is the time for taking the most delicate care that the balances are correct. This every sister of the Bene Gesserit knows.

— from “Manual of Muad’Dib” by the Princess Irulan, *Dune* [16]

This chapter contains the implementation of the algorithms from Ch. 2 through 4 in Sec. 5.2 to 5.4, the generation of the datasets used by the algorithms in Sec. 5.1, the visualisation of reconstruction results in Sec. 5.5 and the error quantification of these results in Sec. 5.6. The GitHub repository containing the software used in this report can be found at: https://github.com/aemiliusRetiarius/skripsi_2021.

5.1. Dataset Generation

For the testing purposes of this report, a virtual reference cube is constructed with 98 numbered points on its surface, such that every face has a grid of 5×5 points. This cube is visualised using the alpha shape (defined in Sec. 5.5) and the scatter plot of these points in Fig. 5.1a and 5.1b.



(a) Alpha Shape of Reference Object

(b) Numbered Surface Points on Reference Object

Figure 5.1: Reference Object and Surface Points for Testing

From this set of true points a list of measurements can be taken according to a set of

parameters to simulate the act of observing a physical object. These parameters include the amount of connections per point, the noise added to the measurements and the percentage of records that are corrupted.

Using the Python NumPy [21] and pandas [22] libraries, the algorithm to generate this list of measurements is given below in Al. 4.2.

The format of the distance list is given in the Tab. 5.1 below. Note that the **Tolerance** column gives the standard deviation of the Gaussian noise added to the measurement and the **Changed** column contains a Boolean value that flags corrupted records.

Index	Source	Target	Distance	Tolerance	Changed
0	1	8	55.89	0.56	False
1	1	14	90.38	0.90	False
...
246	86	98	102.54	1.03	False

Table 5.1: Example Distance Measurements List

5.2. Deterministic Reconstruction Algorithm Implementation

The implementation of this algorithm is based on the flowchart in Fig. 2.1 and its pseudocode is given in App. E. The software has been written in Python using the NumPy [21], pandas [22], SciPy [23] and scikit-learn [24] libraries and makes calls to Matlab to execute the script in App. C.

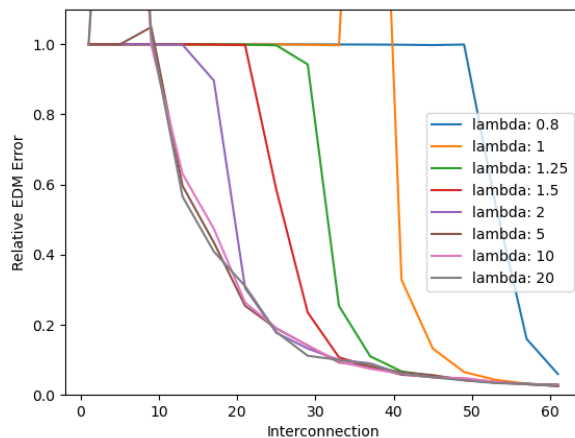


Figure 5.2: Deterministic Algorithm Error for Various Data Fidelity (λ) Values. Note that for higher values of λ , the deterministic algorithm can achieve similar reconstruction error with less measurements per point, up to approximately $\lambda = 10$. After this, the algorithm gives diminishing returns.

Recall from Sec. 2.3 that the semidefinite relaxation script proposed by Dokmanić *et al.* [9] contains the data fidelity term λ proposed by Biswas *et al.* [11]. The value of this term is determined experimentally. The relative EDM error (as defined in Sec. 5.6) versus interconnection for various values of λ is plotted in Fig. 5.2.

It is clear from this figure that the network can perform reconstructions with less data (lower interconnection value) for higher values of λ , up to a certain point. This point seems to be the value $\lambda = 10$ and is the value used in this report. It is a point of possible further research to investigate whether this value holds for more general reconstruction problems or how the problem parameters affects this value.

It is an interesting point to note that this algorithm can work with no prior knowledge of the positions of the true points (as opposed to the probabilistic algorithm that requires a prior distribution of the point positions), however this only produces a reconstruction up to translation, rotation and reflection as seen in Fig. 5.3. In some cases, where only EDM reconstruction is required, this may be an advantage when compared against the probabilistic algorithm which requires at least 3 known points to function.

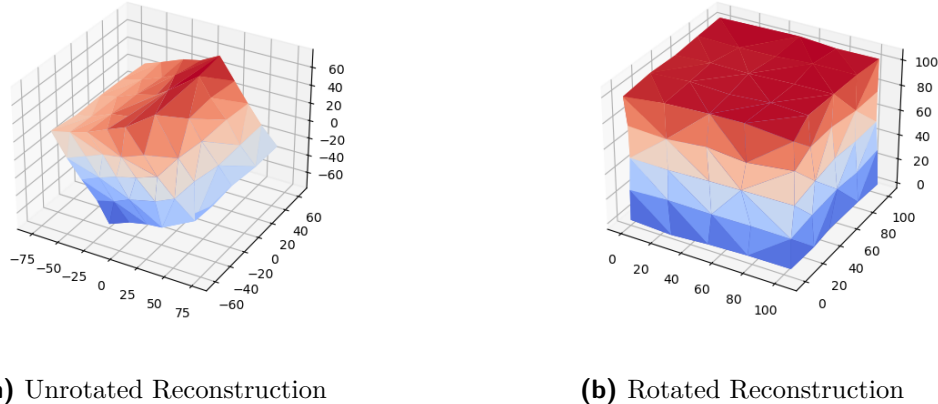


Figure 5.3: Unrotated- and Rotated Deterministic Reconstructions

5.3. Probabilistic Reconstruction Algorithm Implementation

The implementation of this algorithm is based on the flowchart in Fig. 3.1 and its pseudocode is given in App. F. The software has been written in C/C++ using routines and structures from the proprietary PGM library EMDW.

A visualisation of the three steps at each iteration of this algorithm is given below in Fig. 5.4 (note that the observed distances are given by the dashed lines). These steps, in summary, are as follows:

1. Initialise factors from prior positions and connections defined in the distance list.
2. Update factor positions using the UT and the observed distances.
3. Infer new positions and update the prior for the next iteration.

Figure 5.4: Simplified Probabilistic Algorithm Iteration Example¹. In this example, the true, observed measurements are given by the dashed lines between the points. Observe how the inter-point distances more closely reflect these measurements after one iteration.

This software creates a PGM using the dataset generated according to Sec. 5.1 and iteratively applies this to a list of prior positions (formatted as seen in Tab. 5.2) until convergence.

Index	Point_Num	X_Pos	Y_Pos	Z_Pos	X_Tol	Y_Tol	Z_Tol
0	1	0	0	0	0	0	0
1	2	31.74	7.38	11.58	10	10	10
...
97	98	88.65	25.69	10.27	10	10	10

Table 5.2: Example Prior/Result Positions List

This list of positions represents the prior knowledge the algorithm receives regarding the positions of the points. For testing purposes, Gaussian noise is added to the true positions

¹Requires Adobe Acrobat or Okular PDF viewer to display animation.

(with the standard deviation of this noise given in the **Tol** columns in Tab. 5.2) to simulate different levels of accuracy for this prior knowledge. If prior positions are not given, the positions are initialised randomly in predefined cube.

Dimensions with positions that are observed are represented in the list of positions by setting their values to the true values and the corresponding tolerance/standard deviation to zero. This is seen in the first record of Tab. 5.2, where this point has been chosen as the origin with all of its coordinates observed to be zero. It is important to note that this algorithm requires the positions of 3 observed points (excluding the origin) to function². However, this nullifies the need for the rotation correction of the deterministic algorithm of Sec. 5.2.

In order to avoid the numerical issues mentioned in Sec. 3.2, an additional damping factor λ is added³. At each step where the UT is applied, the new variance is limited to the maximum of the new variance and the old variance multiplied by λ . This ensures that the system does not converge to sub-optimal positions too quickly and that the variances of the points do not underflow.

Convergence for this algorithm is calculated by taking the absolute difference of the positional beliefs at the start and end of each iteration. Once this difference is below a certain threshold, the system has converged. For this report, convergence is declared once the positions have reached 1% of their true positions (absolute difference of 294).

5.4. Error Identification Heuristic Implementation

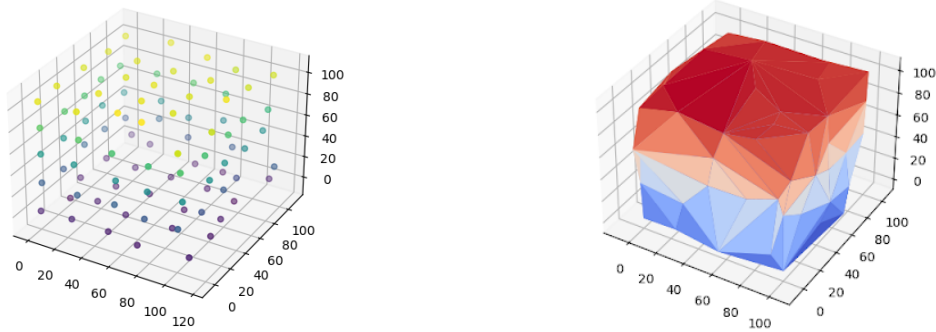
The implementation of this algorithm is based on the flowchart in Fig. 4.1 and its pseudocode is given in App. E. The software has been written in Python using the pandas [22] library.

5.5. Result Visualisation

Both of the algorithms from Sec. 5.2 and 5.3 return a set of 98 3-dimensional reconstructed points $\hat{\mathbf{X}}$. These points can be visualised using a simple scatter plot (Fig. 5.5a), but it can be hard to get a sense of the shape of the reconstructed object given the lack of depth in the image. To help in this regard, an alpha shape is constructed using these points and the Alpha Shape Toolbox Python library [25] as seen in Fig. 5.5b.

²Since a 4 points are needed to orient a 3-dimensional volume with no ambiguity.

³Through trial and error, the value of $\lambda = 0.8$ seems to work in the most circumstances. This may be due to its proximity to the optimal damping ratio ($\frac{1}{\sqrt{2}}$) but no testing has been done to support this intuition.

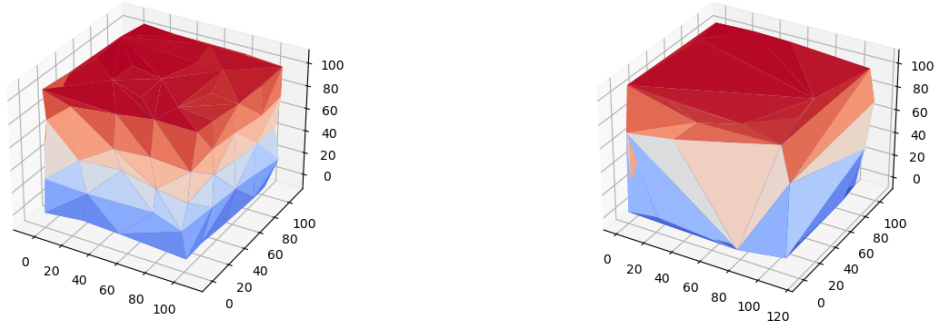


(a) Scatter Plot of Reconstructed Points Example **(b)** Alpha Shape of Reconstruction Example

Figure 5.5: Scatter and Alpha Shape Plot Examples

An alpha shape is defined as a minimum bounding polytope of a set of points [26], in a sense the "shape" that would be obtained by stretching a rubber band around all of the points.

This method of visualisation requires the tuning of an α -parameter, from which the name "alpha shape" derives, which sets how aggressively the shape is minimised by limiting the maximum length of the sides of the polytope. If this parameter is set too high, the process will fail and if it is set too high, surface detail may be lost (Fig. 5.6b as opposed to Fig. 5.6a). A simple heuristic to determine this value would be to take the reciprocal of the average distance between the reconstructed points, although this has not been extensively tested⁴.



(a) Suitable $\alpha = 0.01$

(b) Excessive $\alpha = 0.001$

Figure 5.6: Alpha Shapes with Suitable and Excessive Values for α . Note the lack of surface detail on Fig. 5.6b as opposed to Fig. 5.6a.

⁴The value of $\alpha = 0.01$ used in the visualisations of this report was determined through trial and error, but roughly follows this heuristic.

5.6. Error Quantification

To provide an objective and quantised measure of the error of the reconstruction, a measure is required that is decoupled from the subjective measure of visual fidelity. The measure of relative Euclidean distance matrix error, as used by Dokmanić *et al.* [9], is used in this report.

This measure uses the EDM of the true points (\mathbf{D}) and the EDM of the reconstructed points ($\hat{\mathbf{D}}$) and compares the two. It is defined by the following equation:

$$\text{err}_{\text{rel}} = \frac{\|\hat{\mathbf{D}} - \mathbf{D}\|_F}{\|\mathbf{D}\|_F} \quad (5.1)$$

This provides a way to measure the reconstruction performance without needing to first correct the orientation of the reconstruction, since the EDM is the same for all orientations of the reconstruction.

Broadly, the behaviour of the err_{rel} with respect to the connections per point (interconnections) follows the pattern in Fig. 5.7, with an initial plateau, a large spike and a descent to a converged value. As a good rule of thumb, reconstructions with an error of less than 0.1 can be regarded as good reconstructions.

The corresponding alpha shapes of reconstructions in these regions will be similar to those also given in Fig. 5.7.

Figure 5.7: Reconstruction Behaviour Example⁵.

⁵Requires Adobe Acrobat or Okular PDF viewer to display animation.

Chapter 6

Experimental Results

KULL WAHAD!: “I am profoundly stirred!” A sincere exclamation of surprise common in the Imperium. Strict interpretation depends on context. (It is said of Muad’Dib that once he watched a desert hawk chick emerge from its shell and whispered: “Kull wahad!”)

— Terminology of the Imperium, *Dune* [16]

This chapter compiles the results of the reconstructions obtained from the algorithms from Ch. 2 and 3 using the testing framework of Ch. 5.

In the context of these results, the noise percentage added to the distance measurements during the dataset generation refers to the 3.5σ boundary of the added zero-mean Gaussian noise as a percentage of the measurement. Additionally, the error percentage refers to the percentage of records that have been corrupted by changing either the source point, target point or the measured distance.

Also note that the relative EDM error, as defined in 5.6, has been clipped to 1.1 in all of the graphs to ensure better readability and that all data points are the average error of at least four executions of the respective algorithms with randomly generated datasets.

The relative speed of the algorithms is not tested in this report. It would not be fair to compare the algorithms by this metric, as the speed of the algorithms is very dependent on their initial parameters (such as the data fidelity term for the deterministic algorithm or the damping factor for the probabilistic algorithm, both of which have a significant effect on execution time) and finding values for these parameters for an equal comparison is a subjective exercise. The implementation of these algorithms have also been optimised to different levels, owing to the different libraries used. For a fair comparison, bespoke software would have to be written that could be optimised to the furthest extent possible.

6.1. Deterministic Algorithm Performance

This section serves to illustrate the performance of the deterministic algorithm of Ch. 2 by calculating the error of the reconstructions, as defined by the experimental framework of Ch. 5.

Firstly, the error for different interconnection (number of connections per point that are measured) values along with the noise percentage (as defined in the introduction of the chapter) added to the measurements are given in Fig. 6.1:

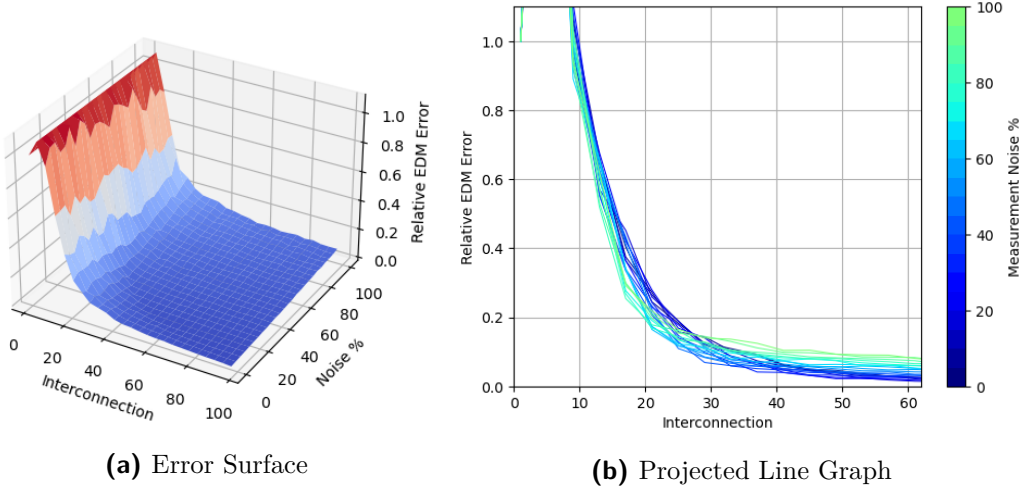


Figure 6.1: Error Surface and Line Graph for Network Interconnection and Measurement Noise Percentage with Deterministic Algorithm

It is clear that the deterministic algorithm is quite robust to Gaussian noise (as speculated in Sec. 2.2), returning good reconstructions even in the presence of large amounts of noise.

Next, the performance of the deterministic algorithm is determined while the presence of record errors (also defined in chapter introduction). This performance is given in Fig. 6.2:

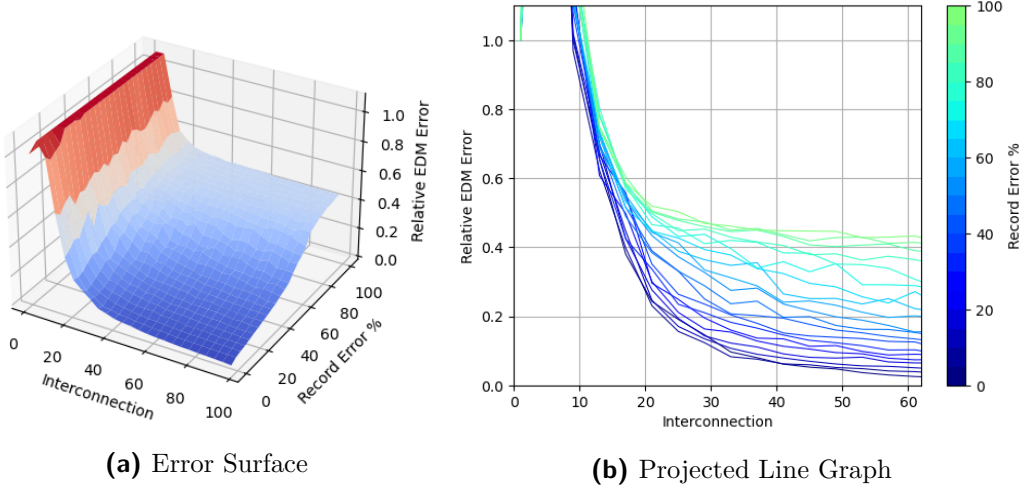
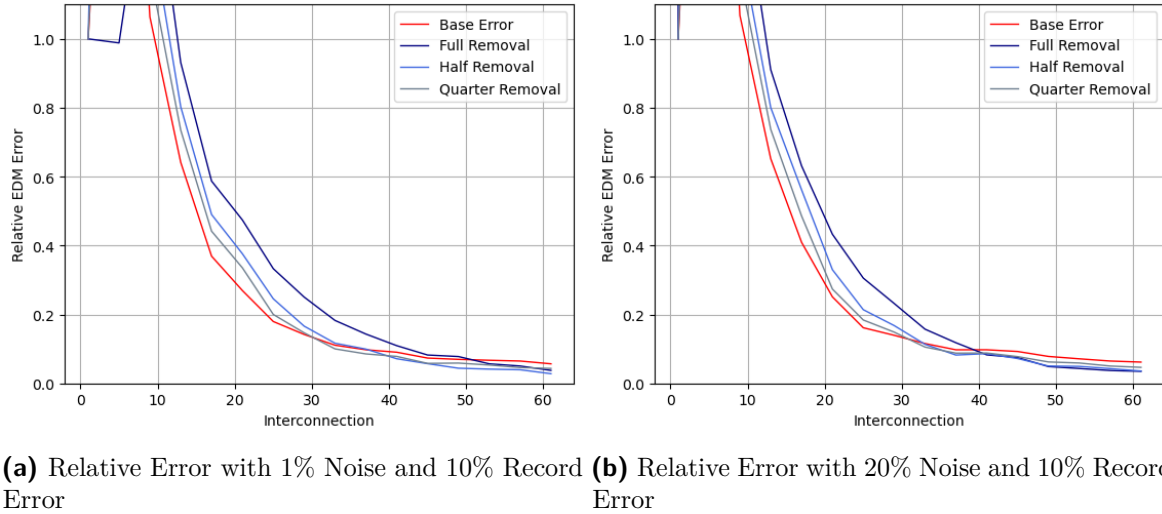


Figure 6.2: Error Surface and Line Graph for Network Interconnection and Record Error Percentage with Deterministic Algorithm

Comparing this figure to Fig. 6.1, it is clear that the deterministic algorithm is more sensitive to record error than measurement noise, no longer returning good reconstructions at around the 40% record error mark.

Using the heuristic error identification algorithm of Ch. 4, the deterministic algorithm is applied to datasets with 10% record error and 1% (Fig. 6.3a) and 10% (Fig. 6.3b) Gaussian measurement noise. These graphs show the reconstruction performance of the deterministic algorithm after various portions of the identified records are removed.



(a) Relative Error with 1% Noise and 10% Record Error **(b)** Relative Error with 20% Noise and 10% Record Error

Figure 6.3: Relative Error of Deterministic Algorithm after Removing Corrupted Records Identified by Heuristic Algorithm

Unfortunately, this heuristic identification method only improves the reconstruction error when more than ≈ 40 connections per point are measured, with 50% removal of identified records offering the best balance. This can result in up to a 50% reduction in the reconstruction error, however, this is only possible when the reconstruction error is already very low, limiting the practical application of this identification method for the deterministic algorithm.

6.2. Probabilistic Algorithm Performance

As a comparison to the previous section, this section shows the performance of the probabilistic algorithm of Ch. 3, also with the experimental framework of Ch. 5.

With Fig. 6.4 and 6.5, the importance of the prior knowledge of the true point positions is shown. It is clear that superior performance is obtained (i.e. lower error across the interconnection axis), with increasingly accurate prior distributions for the point positions yielding better results. This makes intuitive sense as the model has to do less refinement of the point positions during the reconstruction process.

It is also enlightening to note from these figures that the performance obtained using a uniform random distribution for the prior positions (given in red in Fig. 6.4b and 6.5b) is very susceptible to noise, completely failing to achieve good reconstructions when 20% measurement noise is added. This behaviour is also seen in Fig. 6.6.

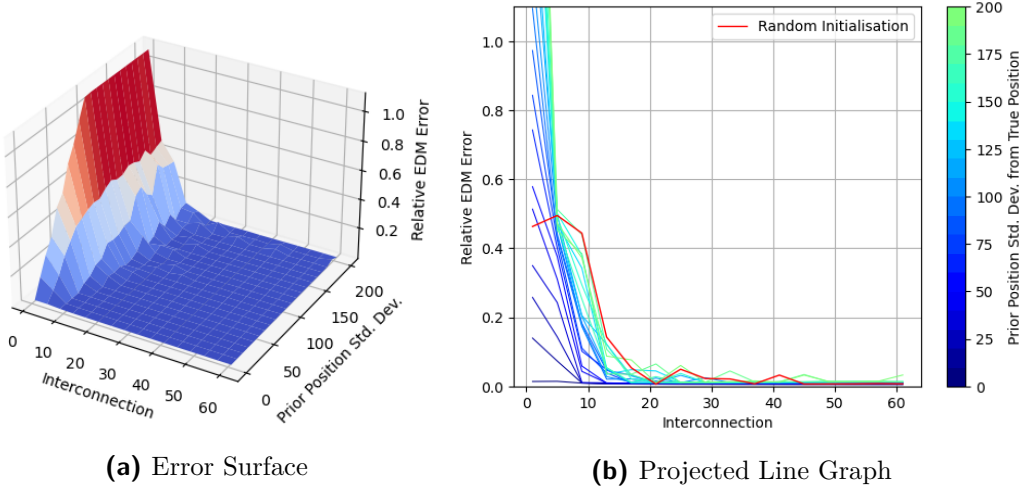


Figure 6.4: Error Surface and Line Graph for Network Interconnection and Positional Prior Standard Deviation with Probabilistic Algorithm (1% Noise)

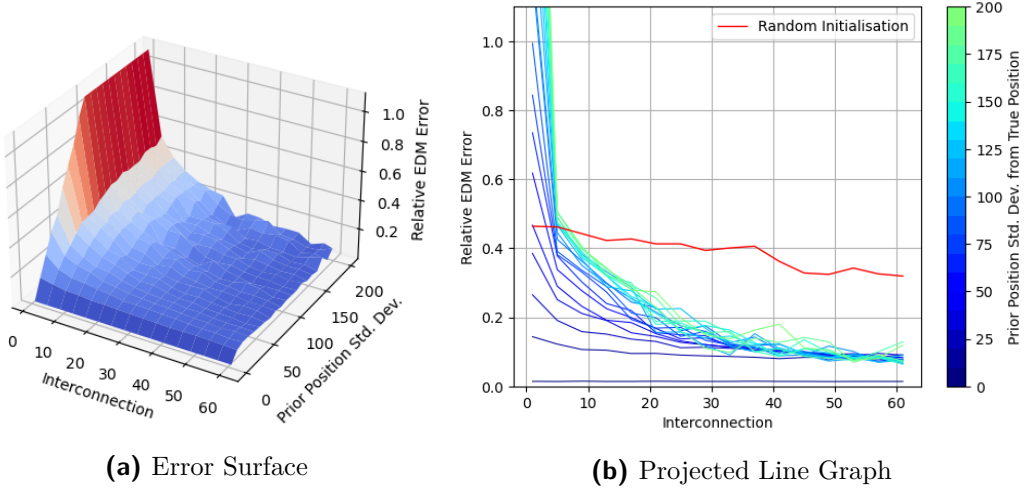


Figure 6.5: Error Surface and Line Graph for Network Interconnection and Positional Prior Standard Deviation with Probabilistic Algorithm (20% Noise)

As mentioned previously, using a uniform random distribution as a prior for the positions of the reconstructed points results in a system that is very sensitive to measurement noise and, by extension, record error. This behaviour is conveyed in Fig. 6.6, where the algorithm only functions effectively with very small measurement noise parameters. The variance of the data points (i.e. the "jaggedness") of the graph may also indicate that the system is very unstable, converging to good solutions only periodically. This behaviour may be due to the fact that the probabilistic system struggles to reorient the points that have been randomly initialised¹.

¹In some sense, the prior is actively resisting the attempts of the probabilistic algorithm to move the points *away* from the inaccurate and unoriented prior.

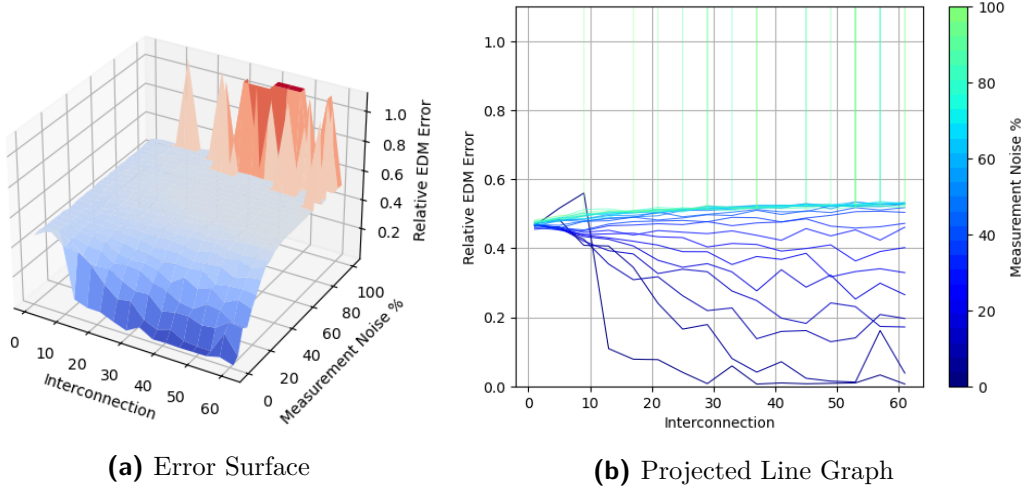


Figure 6.6: Error Surface and Line Graph for Network Interconnection and Measurement Noise Percentage with Randomly Initialised Probabilistic Algorithm

For Figure 6.7, 6.8 and 6.9, a prior distribution with a standard deviation of 100 from the true positions is used to investigate the performance of the algorithm with a prior that is not a uniform random distribution.

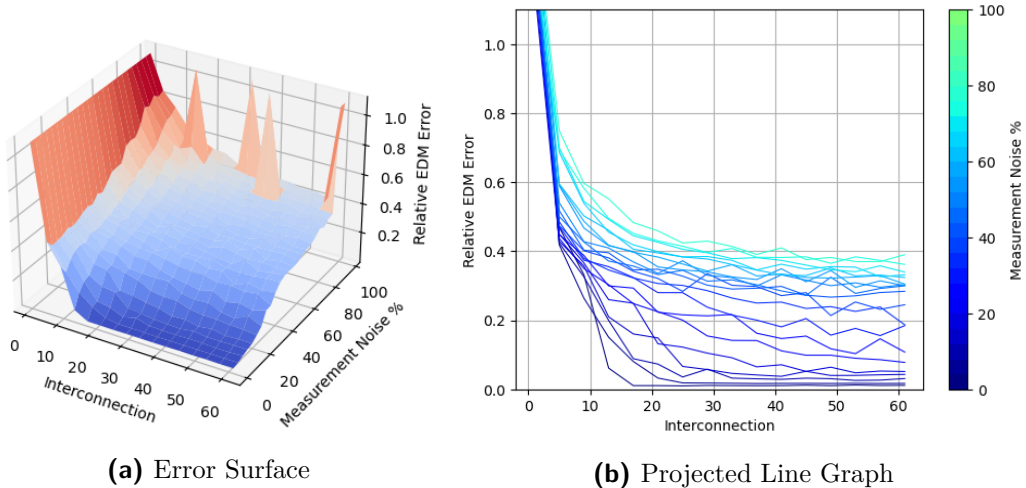


Figure 6.7: Error Surface and Line Graph for Network Interconnection and Measurement Noise Percentage with Probabilistic Algorithm (Prior Standard Deviation = 100)

Comparing Fig. 6.6 and 6.7, it is clear that the latter has superior noise handling characteristics, re-emphasising the value of information regarding the prior distributions. This noise resilience, however, is not as good as that of the deterministic algorithm (as seen in Fig. 6.1), indicating that the deterministic algorithm may yield better reconstructions in very noisy environments.

Fig. 6.8 below also indicates, for the probabilistic algorithm, a similar response to record errors to that of the deterministic algorithm in Fig. 6.2.

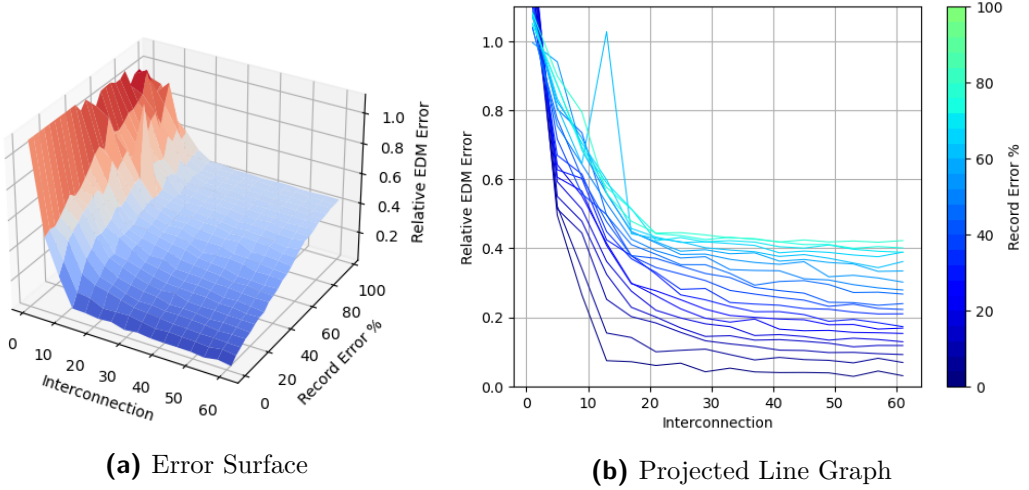


Figure 6.8: Error Surface and Line Graph for Network Interconnection and Record Error Percentage with Probabilistic Algorithm (Prior Standard Deviation = 100)

In a similar fashion to Fig. 6.3, the heuristic error identification algorithm of Ch. 4 and the probabilistic algorithm is applied to datasets with 10% record error and 1% (Fig. 6.3a) and 10% (Fig. 6.3b) Gaussian measurement noise. These graphs show the reconstruction performance of the probabilistic algorithm after various portions of the identified records are removed.

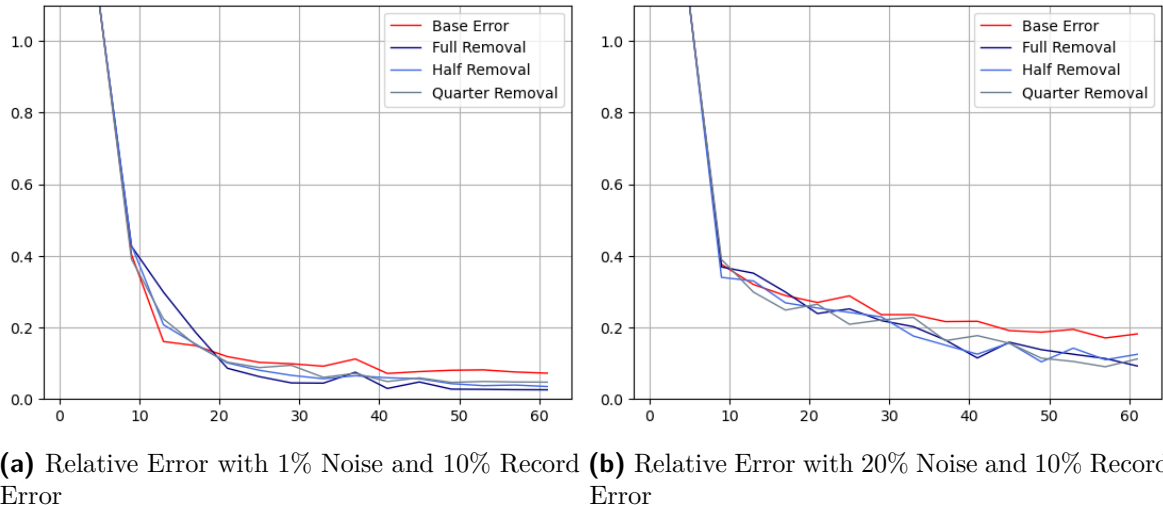


Figure 6.9: Relative Error of Probabilistic Algorithm after Removing Corrupted Records Identified by Heuristic Algorithm

Observing Fig. 6.9, it is clear that the heuristic algorithm provides significant value to the probabilistic algorithm (as opposed to the marginal gains for the deterministic algorithm in Fig. 6.3), consistently reducing, and almost halving in some cases, the reconstruction error. This may be due to the fact that in the evidence-based framework of the probabilistic algorithm, the erroneous measurements have a larger influence on the reconstruction, yielding larger performance gains when removed.

6.3. Performance Comparison

To compare the performance of the deterministic and probabilistic algorithms of Ch. 2 and 3, the reconstruction error is obtained for varying interconnection levels (indicating the amount of data available for the reconstruction) with measurement noise- and error levels that can be expected in practical applications. If an algorithm can achieve the same level of reconstruction error as another for a lower interconnection value (i.e. less data required), it can reasonably be concluded that the algorithm is superior.

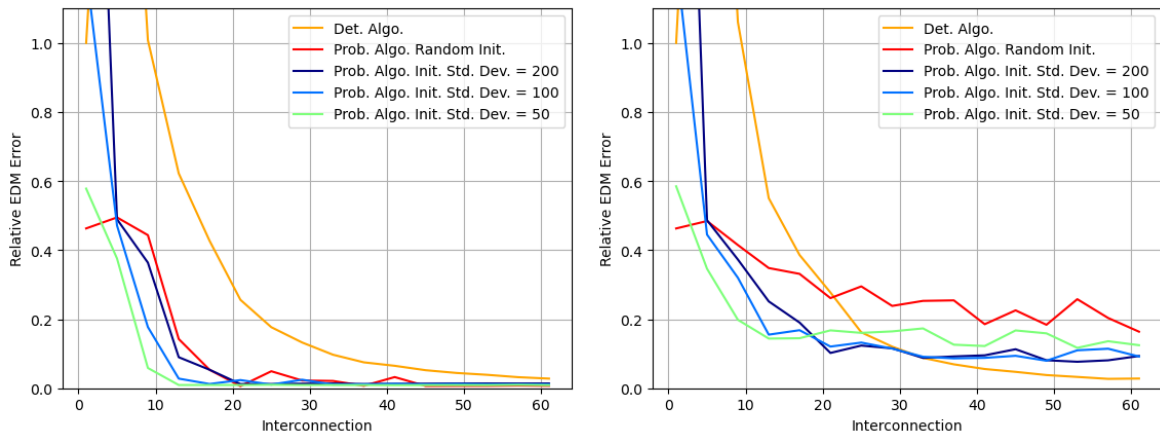


Figure 6.10: Performance Comparison of Deterministic and Probabilistic Reconstruction Algorithms

From Fig. 6.10, it is clear that the probabilistic algorithm displays superior performance to the deterministic algorithm. This is especially true in the case of low noise in Fig. 6.10a, where, even in the worst case of a uniformly random initialisation for the positional prior, the probabilistic algorithm boasts superior performance by every metric.

While not as impressive as the low noise case, the probabilistic algorithm also performs better in the more standard scenario of Fig. 6.10b. In this case, the uniformly random initialisation struggles, restricting its use case to low noise applications.

In Fig. 6.10b, the deterministic algorithm also has a lower steady-state error value for high interconnection levels. Using this fact as well as the noise robustness of the algorithm, as seen in Fig. 6.1, it can be concluded that the deterministic algorithm is the better choice for applications with high measurement availability and high levels of measurement noise.

In summary, the probabilistic algorithm is a viable improvement on the standard deterministic approach to the problem of virtual object reconstruction from paired-point distances in most practical situations.

Chapter 7

Summary and Conclusion

Truth suffers from too much analysis.

— Ancient Fremen saying, *Dune Messiah* [1]

7.1. Summary

The objective for this report has been to develop a probabilistic alternative to the standard deterministic approach to the virtual reconstruction from paired-point distances.

The baseline deterministic algorithm has been constructed on the foundation of the Euclidean distance Matrix (EDM), a description of the inter point distances in matrix form. Using multidimensional scaling (MDS), this matrix is projected to 3-dimensional space to reconstruct the points. While trivial for the case of a fully defined EDM (i.e. every distance between every pair of points is measured), in practical cases only a subset of these measurements are available. The gaps of the EDM are filled using semidefinite programming (SDP), that views EDM completion as an optimisation problem with the available measurements as constraints.

As an alternative based on inference rather than optimisation, a probabilistic algorithm has been designed using the theory of probabilistic graphical models (PGM). This algorithm views the positions of the reconstructed points as a network of probabilistic distributions of random variables. These distributions are shifted to conform to the known distances using the unscented transform (UT) and new positions are inferred using marginalisation of the full joint distribution, a process that is iteratively applied until the positions converge.

The compiled theory of these algorithms are given in Ch. 2 to 4 and the respective software implementations in Ch. 5.

A simple heuristic to identify and remove corrupted measurements, based on the relative change of the measurements during reconstruction, is also proposed to reduce the error of reconstructions.

The performance of these algorithms are tested using datasets generated from a virtual reference cube and the error of the reconstructions are quantified (Ch. 5).

7.2. Conclusion

The results of Sec. 6.3 indicate that the probabilistic algorithm designed in this report outperformed the standard, deterministic algorithm for most practical applications. While the probabilistic algorithm is not as robust to measurement noise and measurement corruption as the baseline algorithm, performance parity is only reached with noise levels in excess of 20%, much noisier than most practical scenarios. The probabilistic algorithm also has the advantage of being able to take advantage of prior information regarding the object to be reconstructed, possibly significantly improving its performance.

The heuristic error identification also yields marginal performance gains when used with the deterministic algorithm and when good amounts of data is available. However, the heuristic error identification is much more effective when used in conjunction with the probabilistic algorithm, yielding markedly less reconstruction error in most cases.

In all, it can be concluded that this report has accomplished the objective of designing and implementing an alternative algorithm to the baseline, deterministic approach to the virtual object reconstruction from paired-point distances problem. This report has also augmented these algorithms with a heuristic method to identify and remove erroneous measurements, improving reconstruction accuracy.

7.3. Future Work

- Analyse performance of algorithms with more reference objects to determine more general performance characteristics.
- Investigate impact of problem setup on algorithm hyperparameters, such as investigating how to choose the optimal value for the data fidelity term λ of the deterministic algorithm from Ch. 2.
- Implement probabilistic method of identifying corrupted measurements.
- Implement junction tree/loopy belief propagation algorithm for the probabilistic algorithm of Ch. 3 to handle larger systems of points.
- Optimise implementation of the algorithms from Ch. 2 to 4 test speed characteristics and to handle larger reconstructions.
- Apply probabilistic algorithm to more general EDM completion problems such as the sensor localisation problem from Dokmanić *et al.* [9].

Bibliography

- [1] F. Herbert, *Dune Messiah*. Ace, 1969.
- [2] J. Dattorro, *Convex Optimization Euclidean Distance Geometry*. Meboo Publishing USA, 2005, ch. 5. [Online]. Available: <https://books.google.co.za/books?id=VxuRF4NhjykC>
- [3] W. Kaplan, *Maxima and Minima with Applications: Practical Optimization and Duality*, ser. Wiley Series in Discrete Mathematics and Optimization. Wiley, 2011, pp. 61–62. [Online]. Available: <https://books.google.co.za/books?id=bAo6KNZcUP0C>
- [4] J. C. Gower, “Euclidean distance geometry,” *Mathematical Scientist*, vol. 7, pp. 1–14, 1982.
- [5] W. Torgerson, “Multidimensional scaling: I. theory and method.” *Psychometrika*, vol. 17, p. 401–419, 1952. [Online]. Available: <https://doi.org/10.1007/BF02288916>
- [6] F. Wickelmaier, *An introduction to MDS*, ser. Aalborg Universitetscenter. Institut for Elektroniske Systemer. Afdeling for Kommunikationsteknologi. Rapport. Aalborg Universitetsforlag, 2003, no. R00-6003, p. 10.
- [7] A. Buja, D. Swayne, M. Littman, N. Dean, H. Heike, and L. Chen, “Data visualization with multidimensional scaling,” *Journal of Computational and Graphical Statistics*, vol. 17, pp. 444–472, Jun. 2008. [Online]. Available: <https://doi.org/10.1198/106186008X318440>
- [8] E. Peterfreund and M. Gavish, “Multidimensional scaling of noisy high dimensional data,” 2018. [Online]. Available: <https://doi.org/10.1016/j.acha.2020.11.006>
- [9] I. Dokmanić, R. Parhizkar, J. Ranieri, and M. Vetterli, “Euclidean distance matrices: Essential theory, algorithms, and applications,” *IEEE Signal Processing Magazine*, vol. 32, no. 6, pp. 12–30, 2015. [Online]. Available: <https://doi.org/10.1109/MSP.2015.2398954>
- [10] N. Krislock and H. Wolkowicz, *Euclidean Distance Matrices and Applications*. Boston, MA: Springer US, Jan. 2012, pp. 879–914. [Online]. Available: https://doi.org/10.1007/978-1-4614-0769-0_30

- [11] P. Biswas, T.-C. Liang, K.-C. Toh, Y. Ye, and T.-C. Wang, “Semidefinite programming approaches for sensor network localization with noisy distance measurements,” *IEEE Transactions on Automation Science and Engineering*, vol. 3, no. 4, pp. 360–371, 2006. [Online]. Available: <https://doi.org/10.1109/TASE.2006.877401>
- [12] MATLAB, *version 9.11 (R2021b)*. Natick, Massachusetts: The MathWorks Inc., 2021.
- [13] M. Grant and S. Boyd, “Cvx: Matlab software for disciplined convex programming, version 2.1.” Mar. 2014. [Online]. Available: <http://cvxr.com/cvx>
- [14] W. Kabsch, “A solution for the best rotation to relate two sets of vectors,” *Acta Crystallographica Section A*, vol. 32, no. 5, pp. 922–923, Sep. 1976. [Online]. Available: <https://doi.org/10.1107/S0567739476001873>
- [15] A. S. Householder, “Unitary triangularization of a nonsymmetric matrix,” *Journal of the ACM*, vol. 5, no. 4, p. 339–342, Oct. 1958. [Online]. Available: <https://doi.org/10.1145/320941.320947>
- [16] F. Herbert, *Dune*. Chilton Books, 1965.
- [17] R. Trudeau, *Introduction to Graph Theory*, ser. Dover Books on Mathematics. Dover Publications, 2013. [Online]. Available: <https://books.google.gg/books?id=eRLEAgAAQBAJ>
- [18] D. Barber, *Bayesian Reasoning and Machine Learning*, ser. Bayesian Reasoning and Machine Learning. Cambridge University Press, 2012. [Online]. Available: https://books.google.co.za/books?id=yxZtddB_0b0C
- [19] D. Koller and N. Friedman, *Probabilistic Graphical Models: Principles and Techniques*, ser. Adaptive computation and machine learning. MIT Press, 2009. [Online]. Available: <https://books.google.co.za/books?id=7dzpHCHzNQ4C>
- [20] S. J. Julier and J. K. Uhlmann, “New extension of the Kalman filter to nonlinear systems,” in *Signal Processing, Sensor Fusion, and Target Recognition VI*, I. Kadar, Ed., vol. 3068, International Society for Optics and Photonics. SPIE, 1997, pp. 182 – 193. [Online]. Available: <https://doi.org/10.1117/12.280797>
- [21] NumPy, *version 1.21.1*. Community Project, 2021. [Online]. Available: <https://numpy.org/>
- [22] pandas, *version 1.3.0*. Wes McKinney, 2021. [Online]. Available: <https://pandas.pydata.org/>
- [23] SciPy, *version 1.7.1*. Community Project, 2021. [Online]. Available: <https://scipy.org/>

- [24] scikit learn, *version 1.0.1*. Community Project, 2021. [Online]. Available: <https://scikit-learn.org/>
- [25] A. S. Toolbox, *version 1.3.1*. Kenneth E. Bellock, 2021. [Online]. Available: <https://pypi.org/project/alphashape/>
- [26] H. Edelsbrunner, D. Kirkpatrick, and R. Seidel, “On the shape of a set of points in the plane,” *IEEE Transactions on Information Theory*, vol. 29, no. 4, pp. 551–559, 1983. [Online]. Available: <https://doi.org/10.1109/TIT.1983.1056714>

Appendix A

Project Planning Schedule

Week	Date	Planned Progress
1	08/08/2021	Familiarise with problem
2	15/08/2021	Do literature review of deterministic methods (MDS, SDP)
3	22/08/2021	Do literature review of probabilistic methods (PGMs, UT)
4	29/08/2021	Implement deterministic algorithm
5	05/09/2021	Add testing framework for algorithms
6	12/09/2021	Add parallel execution functionality
7	19/09/2021	Obtain results from deterministic algorithm
8	26/09/2021	Implement probabilistic algorithm
9	03/10/2021	Obtain results from probabilistic algorithm
10	10/10/2021	Compile literature review in report
11	17/10/2021	Compile implementation in report
12	24/10/2021	Compile results in report
13	31/10/2021	Incorporate feedback
14	07/11/2021	Finalise Report

Table A.1: Project Schedule per Week

Appendix B

Outcomes Compliance

Outcomes	Chapters	Justification
ELO 1: Problem solving	1, 2, 3, 4	Identifying the reconstruction problem, solving the reconstruction problem from paired point distances using the theory from deterministic/probabilistic methods.
ELO 2: Application of scientific and engineering knowledge	2, 3, 4, 5	Application of abstract concepts from linear algebra, statistics, and probabilistic theory in designing algorithms to solve the reconstruction problem, including Euclidean distance matrices, multidimensional scaling, semidefinite programming, probabilistic graphical models, and the unscented transform.
ELO 3: Engineering Design	2, 3, 4, 5	In the implementation of the designed algorithms, various concepts are synthesized using non-procedural methods. The various abstract concepts are brought together to design novel procedures that use each of these concepts sequentially to return the desired results. This report contains the metrics and experimental framework to test the algorithms designed as well as the data analysis and presentation of these results obtained from this framework.
ELO 4: Investigations, experiments and data analysis	5, 6	
ELO 5: Engineering methods, skills and tools, including Information Technology	5, 6	Various engineering tools and skills have been used during this report, from software such as Python, C++ and MATLAB, mathematics during the algorithm design to presentation tools such as LATEX for this report.
ELO 6: Professional and technical communication	All chapters	This report in its entirety displays evidence of effective competence in professional and technical communication skills. This evidence is supplemented by the oral- and poster presentations that are to be presented.
ELO 8: Individual work	All chapters	All work contained in this report has been done alone by E. Visser, with advice from weekly consultations with supervisor Prof. J. du Preez. External sources required have been cited fully.
ELO 9: Independent learning ability	All chapters	The theory required for this report is not covered in the standard engineering curriculum and had to be self-taught and researched. Additional skills such as MATLAB and C++ also had to be acquired individually.

Table B.1: ECSA Outcomes Compliance

Appendix C

Matlab/CVX Script for Semidefinite Relaxation

This appendix contains the Matlab/CVX script [12] [13] used to solve the SDP-problem in Sec. 2.3. The script as written by Dokmanić *et al.* [9] can be found below:

```
1 function [EDM, X] = semidefiniteRelaxation(D, W, lambda)
2
3 n = size(D, 1);
4 x = -1/(n + sqrt(n));
5 y = -1/sqrt(n);
6 V = [y*ones(1, n-1); x*ones(n-1) + eye(n-1)];
7 e = ones(n, 1);
8
9 cvx_begin sdp
10     variable G(n-1, n-1) symmetric;
11     B = V*G*V';
12     E = diag(B)*e' + e*diag(B)' - 2*B;
13     maximize trace(G) ...
14         - lambda * norm(W .* (E - D), 'fro');
15     subject to
16         G >= 0;
17 cvx_end
18
19 [U, S, V] = svd(B);
20 EDM = diag(B)*e' + e*diag(B)' - 2*B;
21 X = sqrt(S)*V';
```

Appendix D

Dataset Generation Algorithm Pseudocode

Algorithm 4.2: Distance Measurements List Generation

Input: numPoints, reqCons, noisePercent, errorPercent

Output: distList

```
function GETVALIDPOINTS( $s$ , numPoints, reqCons)
    for  $t \leftarrow 1$  to numPoints do
        if  $s \neq t$  and  $\text{CONS}(t) < \text{reqCons}$  then
            validSet  $\leftarrow$  validSet.APPEND( $t$ )
        end if
    end for
    return validSet
end function

for  $s \leftarrow 1$  to numPoints do
    if  $\text{CONS}(s) < \text{reqCons}$  then
        validSet  $\leftarrow$  GETVALIDPOINTS( $s$ , numPoints, reqCons)
         $t \leftarrow \text{PICKRAND}(\text{validSet})$ 
         $d \leftarrow \text{GETDIST}(s, t)$ 
         $d \leftarrow \text{GAUSSIANNOISE}(d, \text{noisePercent})$ 
        distList  $\leftarrow$  distList.APPEND( $s, t, d$ )
    end if
end for

for  $s \leftarrow 1$  to  $\text{numPoints} * \text{errorPercent}$  do
    if  $\text{CONS}(s) < \text{reqCons}$  then
        validSet  $\leftarrow$  GETVALIDPOINTS( $s$ , numPoints, reqCons)
        record  $\leftarrow \text{PICKRAND}(\text{distList})$ 
        record  $\leftarrow \text{CORRUPT}(\text{record})$ 
        distList  $\leftarrow$  distList.UPDATE(record)
    end if
end for

return distList
```

Appendix E

Deterministic Reconstruction Algorithm Pseudocode

Algorithm 5.3: Deterministic Reconstruction Implementation

Input: distList

Output: recPoints

```
numPoints ← MAX(MAX(distList[”Source”]), MAX(distList[”Target”]))  
maskMat, edmMatRaw ← NUMPY.ZEROS((numPoints, numPoints))  
truePoints ← GETREFERENCEPOINTS(numPoints)  
  
for  $i \leftarrow 1$  to distList.len do  
     $s \leftarrow \text{disList}[i][”Source”]$   
     $t \leftarrow \text{disList}[i][”Target”]$   
    maskMat[ $s, t$ ], maskMat[ $t, s$ ] ← 1  
    edmMatRaw[ $s, t$ ], edmMatRaw[ $t, s$ ] ← disList[i][”Distance”]  
end for  
  
edmMatRec ← CALLMATLABFUNCTION(SEMIDEFRELAXATION(edmMatRaw,  $\lambda = 10$ ))  
resPoints ← SKLEARN.MANIFOLDS.MDS(edmMatRec, components= 3)  
  
truePoints ← truePoints - truePoints[0, :]  
resPoints ← resPoints - resPoints[0, :]  
trueSubset ← TAKESUBSET(truePoints, 3)  
resSubset ← TAKESUBSET(resPoints, 3)  
trueCross ← NUMPY.CROSS(trueSubset[1, :], trueSubset[2, :])  
trueCrossNormed ← trueCross/NUMPY.NORM(trueCross)  
resCross ← NUMPY.CROSS(resSubset[1, :], resSubset[2, :])  
resCrossNormed ← resCross/NUMPY.NORM(resCross)  
trueDot ← NUMPY.CROSS(trueCrossNormed, trueSubset[3, :])  
trueDotNormed ← trueDot/NUMPY.NORM(trueDot)  
resDot ← NUMPY.CROSS(resCrossNormed, resSubset[3, :])  
resDotNormed ← resDot/NUMPY.NORM(resDot)
```

```
if NUMPY.SIGN(trueDotNormed) ≠ NUMPY.SIGN(resDotNormed) then
    householder ← IDENTITY(3) - 2*NUMPY.DOT(resCrossNormed.T, resCrossNormed)
    resPoints
    resPoints ← NUMPY.DOT(resPoints, householder)
end if

rotMat ← SCIPY.SPATIAL.TRANSFORM.ROTATION.ALIGN_VECTORS(trueSubset, resSubset)
resPoints ← NUMPY.DOT(resPoints, rotMat)
return resPoints
```

Appendix F

Probabilistic Reconstruction Algorithm Pseudocode

Algorithm 6.4: Probabilistic Reconstruction Implementation

Input: distList, tolerance, observations, prior_positions (optional)

Output: recPoints

```
function INITCLUSTERS(distList, positions)
    for dist in distList do
        s ← dist[”Source”]
        t ← dist[”Target”]
        cluster ← add postions[s] to cluster
        cluster ← add positions[t] to cluster
        Add cluster to clusterList
    end for
    return clusterList
end function

function APPLYUT(distList, clusterList)
    for (dist, cluster) in (distList, clusterList) do
        sigmaPoints ← sample sigma points from cluster
        sigmaPoints ← add dimesion using Euclidean distance
        cluster ← reconstruct cluster from sigma points
        cluster ← observe cluster using measurement from dist
    end for
    return clusterList
end function
```

```

function INFERNEWPos(clusterList)
    joint ← multiply clusters to obtain joint
    for point in Points do
        positions ← marginalize joint and take MAP estimate for new point coords
        positions ← limit tol to max of new tol and ( $\lambda = 0.8$ ) * old tol
    end for
    return positions
end function

numPoints ← MAX(MAX(distList["Source"]), MAX(distList["Target"]))
if Prior positions given then
    priorfactors ← prior_positions
else
    priorfactors ← init prior positions randomly
end if
positions ← set observed values and set their tol to zero
while change > (tolerance = 294) and iter < (iter_lim = 25) do
    old_positions ← store current positions
    clusterList ← INITCLUSTERS(distList, positions)
    clusterList ← APPLYUT(distList, clusterList)
    positions ← INFERNEWPos(clusterList)
    change ← old_positions - positions
    iter ← iter + 1
    prior_positions ← positions (prior for next iteration)
end while
recPoints ← positions
return recPoints

```

Appendix G

Heuristic Error Identification Algorithm Pseudocode

Algorithm 7.5: Heuristic Error Identification

Input: distList, recPoints, errPerc

Output: distListReduced

```
for dist in distList do
    s ← dist[”Source”]
    t ← dist[”Target”]
    newDist ← DIST(recPoints[s], recPoints[t])
    dist[”Change”] ← (dist[”Dist”] - newDist) / dist[”Dist”]
end for
distList ← Sort by ”Change” column ascending
distListReduced ← Remove first errPerc * length(distList) records from distList
return distListReduced
```
